This Accepted Manuscript has not been copyedited and formatted. The final version may differ from this version.

eNeuro

Research Article: New Research | Cognition and Behavior

AhR Deletion Promotes Aberrant Morphogenesis and Synaptic Activity of Adult-Generated Granule Neurons and Impairs Hippocampus-Dependent Memory

Juan de la Parra[1], María I. Cuartero[1], Alberto Pérez-Ruiz[1], Alicia García-Culebras[1], Ricardo Martín[2], José Sánchez-Prieto[2], Juan M. García-Segura[3], Ignacio Lizasoain[1] and María A. Moro[1]

[1]*Unidad De Investigación Neurovascular, Dpto. Farmacología y Toxicología, Facultad De Medicina, and Instituto Universitario De Investigación En Neuroquímica (IUIN), Universidad Complutense De Madrid (UCM); Instituto De Investigación Hospital 12 De Octubre (i+12), Madrid Spain*

[2]*Departamento De Bioquímica y Biología Molecular, Facultad De Veterinaria and IUIN, UCM, Madrid Spain*

[3]*Departamento De Bioquímica y Biología Molecular, Facultad De Ciencias Químicas, and IUIN, UCM, Madrid Spain*

DOI: 10.1523/ENEURO.0370-17.2018

Received: 30 October 2017

Revised: 5 July 2018

Accepted: 9 July 2018

Published: 30 July 2018

Author Contributions: JdlP, MIC and MAM designed research; JdlP, MIC, APR, AGC, RM performed research; JDLP, MIC, RM, JSP, JMGS, IL, MAM analyzed data; JdlP, MIC, MAM wrote the paper.

Funding: Spanish Ministry of Economy and Competitiveness
SAF2015-68632-R
SAF2016-81716-REDC

Funding: Instituto de Salud Carlos III and Fondo Europeo de Desarrollo Regional (FEDER)
RETICS RD16/0019/0009

Funding: http://doi.org/10.13039/501100004587MINECO | Instituto de Salud Carlos III (ISCIII)
PI17/01601

Funding: http://doi.org/10.13039/501100008433Consejería de Educación, Juventud y Deporte, Comunidad de Madrid (Ministry of Education, Youth and Sports, Government of Madrid)
B2017/BMD-3688

Conflict of Interest: Author reports no conflict of interest.

This work was supported by grants from Spanish Ministry of Economy and Competitiveness SAF2015-68632-R (MAM) and SAF2016-81716-REDC (MAM), from Instituto de Salud Carlos III and cofinanced by Fondo Europeo de Desarrollo Regional (FEDER) «Una manera de hacer Europa» PI17/01601 (IL) and RD16/0019/0009 (IL), and from Regional Madrid Government B2017/BMD-3688 (IL).

Contributed equally to this work.

Address correspondence to María A. Moro, Unidad de Investigación Neurovascular, Departamento de Farmacología, Facultad de Medicina, Universidad Complutense, Avenida Complutense s/n, 28040 Madrid, Spain. Tel.: +34-913941452; E-mail: neurona@ucm.es Or María I. Cuartero, Unidad de Investigación Neurovascular, Departamento de Farmacología, Facultad de Medicina, Universidad Complutense, Avenida Complutense s/n, 28040 Madrid, Spain. Tel.: +34-913941452. E-mail: maribel_cd@hotmail.com

Cite as: eNeuro 2018; 10.1523/ENEURO.0370-17.2018

Accepted manuscripts are peer-reviewed but have not been through the copyediting, formatting, or proofreading process.

Copyright © 2018 de la Parra et al.
This is an open-access article distributed under the terms of the Creative Commons Attribution 4.0 International license, which permits unrestricted use, distribution and reproduction in any medium provided that the original work is properly attributed.

eNeuro Accepted Manuscript

Alerts: Sign up at eneuro.org/alerts to receive customized email alerts when the fully formatted version of this article is published.

eNeuro Accepted Manuscript

eNeuro Accepted Manuscript

1 **AhR Deletion Promotes Aberrant Morphogenesis and Synaptic**
2 **Activity of Adult-Generated Granule Neurons and Impairs**
3 **Hippocampus-Dependent Memory**

4

5 Juan de la Parra[1#], María I. Cuartero[1*#], Alberto Pérez-Ruiz[1], Alicia García-
6 Culebras[1], Ricardo Martín[2], José Sánchez-Prieto[2], Juan M. García-Segura[3],
7 Ignacio Lizasoain[1] and María A. Moro[1]*.

8

9 [1]Unidad de Investigación Neurovascular, Dpto. Farmacología y Toxicología,
10 Facultad de Medicina, and Instituto Universitario de Investigación en
11 Neuroquímica (IUIN), Universidad Complutense de Madrid (UCM); Instituto de
12 Investigación Hospital 12 de Octubre (i+12), Madrid, Spain.
13 [2]Departamento de Bioquímica y Biología Molecular, Facultad de Veterinaria
14 and IUIN, UCM, Madrid, Spain.
15 [3]Departamento de Bioquímica y Biología Molecular, Facultad de Ciencias
16 Químicas, and IUIN, UCM, Madrid, Spain.
17 [#]Equal contribution.

18

19 **Author Contributions:** JdlP, MIC and MAM designed research; JdlP, MIC,
20 APR, AGC, RM performed research; JDLP, MIC, RM, JSP, JMGS, IL, MAM
21 analyzed data; JdlP, MIC, MAM wrote the paper.

22

23 ***Address correspondence** to María A. Moro (neurona@ucm.es) or María I.
24 Cuartero (maribel_cd@hotmail.com), Unidad de Investigación Neurovascular,
25 Departamento de Farmacología, Facultad de Medicina, Universidad

eNeuro Accepted Manuscript

26 Complutense, Avenida Complutense s/n, 28040 Madrid, Spain. Tel.: +34-
27 913941452.

28

29 6 figures; 160 words in Abstract; 119 words for Significance Statement; 416
30 words for Introduction; 2114 words for Discussion.

31

32 **Conflict of Interest**: none.

33 **Sources of funding:** This work was supported by grants from Spanish Ministry
34 of Economy and Competitiveness SAF2015-68632-R (MAM) and SAF2016-
35 81716-REDC (MAM), from Instituto de Salud Carlos III and cofinanced by
36 Fondo Europeo de Desarrollo Regional (FEDER) «Una manera de hacer
37 Europa» PI17/01601 (IL) and RD16/0019/0009 (IL), and from Regional Madrid
38 Government B2017/BMD-3688 (IL).

39

eNeuro Accepted Manuscript

40 **ABSTRACT**

41 Newborn granule cells are continuously produced in the subgranular zone of
42 dentate gyrus throughout life. Once these cells mature, they integrate into pre-
43 existing circuits modulating hippocampus-dependent memory. Subsequently,
44 mechanisms controlling generation and maturation of newborn cells are
45 essential for proper hippocampal function. Therefore, we have studied the role
46 of Aryl Hydrocarbon Receptor (AhR), a ligand-activated bHLH-PAS transcription
47 factor, in hippocampus-dependent memory and granule neuronal morphology
48 and function using genetic loss-of-function approaches based on constitutive
49 and inducible-nestin $AhR^{-/-}$ mice. The results presented here show that the
50 impaired hippocampus-dependent memory in AhR absence is not due to its
51 effects on neurogenesis but to aberrant dendritic arborisation and to an
52 increased spine density albeit with a lower number of mature mushrooms
53 spines in newborn granule cells, a finding that is associated to an immature
54 electrophysiological phenotype. Together, our data strongly suggest that AhR
55 plays a pivotal role in the regulation of hippocampal function, by controlling
56 hippocampal granule neuron morphology and synaptic maturation.

57

58 **SIGNIFICANCE STATEMENT**

59 Hippocampus-dependent memory depends on the generation and maturation of
60 dentate gyrus (DG) newborn granule cells. Aryl Hydrocarbon Receptor (AhR) is
61 a ligand-activated bHLH-PAS transcription factor recently implicated in dendrite
62 branching in the CNS. Since its role in the modulation of dendrite branching and
63 plasticity of adult hippocampal newborn granule neurons and subsequent
64 impact on hippocampus-dependent memory remains unknown, we have

eNeuro Accepted Manuscript

65 undertaken its study using genetic loss-of-function approaches in adult mice.
66 Our study provides evidence indicating that AhR is a regulator of dendrite
67 arborisation and proper synaptic maturation of adult hippocampal newborn
68 neurons and showing its critical role for learning and memory function. These
69 findings point out AhR as a new potent druggable target for the treatment of
70 several cognitive disorders.
71

eNeuro Accepted Manuscript

72 **INTRODUCTION**

73 In the adult mammal brain, the hippocampus is one of the main regions
74 implicated in cognitive function. Throughout life, hippocampal newborn neurons
75 migrate into the granule cell layer to become new dentate granule cells where
76 they integrate synaptically into the pre-existing circuits providing potential
77 substrates for new learning and memories (Altman and Das, 1965;
78 Kempermann et al., 1997; Squire and Zola-Morgan, 1991; van Praag et al.,
79 1999). The correct morphogenesis of these newborn neurons is a critical
80 feature for the adequate function of the hippocampus. Although the aberrant
81 integration of adult newborn granule neurons is able to disrupt cognitive function
82 and is linked to several neurological disorders (Winkle et al., 2016; Zhou et al.,
83 2013), the molecular factors that drive the morphogenesis and maturation of
84 these cells are still quite unknown.

85 The aryl hydrocarbon receptor (AhR), a ligand-activated transcription
86 factor that belongs to the basic Helix-loop-Helix Per-Arnt-Sim (bHLH-PAS)
87 superfamily, has been traditionally studied in association with toxic effects of the
88 environmental pollutants and xenobiotic compounds metabolism and its role in
89 the immune system (Fernandez-Salguero et al., 1995; Fernandez-Salguero et
90 al., 1996; Mandal, 2005; Mulero-Navarro and Fernandez-Salguero, 2016;
91 Murray et al., 2014). However, recent studies across different species suggest
92 other important biological roles of AhR in other systems, as the CNS. In
93 invertebrates, AhR homologs are implicated in dendrite branching in neurons: in
94 *Drosophila*, the loss-of-function of the AhR homolog (*spineless*) promotes more
95 complex dendritic arborisation in sensory neurons (Crews and Brenman, 2006;
96 Kim et al., 2006); in *C. elegans*, *ahr-1* mutant (AhR homolog) neurons also turn

eNeuro Accepted Manuscript

97 into a highly-branched architecture (Smith et al., 2013). In mammals, AhR is
98 expressed in the adult brain (Kimura and Tohyama, 2017) and its constitutive
99 activation drastically reduces dendritic arborisation and aberrant neuronal
100 positioning in cortical pyramidal neurons and olfactory bulb interneurons
101 (Kimura et al., 2016; Kimura et al., 2017; Kimura and Tohyama, 2017). AhR
102 mRNA is also expressed in the dentate gyrus (DG) granule cells of the adult
103 hippocampus (Kimura and Tohyama, 2017). In this area, even though it has
104 been reported that AhR might modulate hippocampal neurogenesis (Latchney
105 et al., 2013), its role in the modulation of dendrite branching and plasticity in
106 adult hippocampal newborn granule neurons remains unknown. Therefore, we
107 have studied the role of AhR in hippocampus-dependent memory and granule
108 neuronal morphology and function using genetic loss-of-function approaches in
109 adult mice. Our data demonstrate that the transcription factor AhR plays a
110 crucial role in hippocampus-dependent function, by controlling dendritic
111 arborisation and dendritic spine growth in granule neurons.
112
113 **METHODS**

114 **Animals and tamoxifen treatment**

115 Experiments were performed in male WT and $AhR^{-/-}$ knockout mice
116 (C57BL/6) at 4, 8 and 14 weeks of age, obtained from Taconic. Both WT and
117 $AhR^{-/-}$ mice were generated by crossing heterozygous $AhR^{+/-}$ mice. $AhR^{f/f}$ mice
118 were acquired from The Jackson Laboratory and were maintained through
119 homozygous breeding pairs. AhR icKO mice (tamoxifen-inducible AhR
120 conditional knockout mice) were generated by crossing $AhR^{f/f}$ mice (Walisser et
121 al., 2005) with nestin-Cre^{ERT2} mice (Imayoshi et al., 2008) and then maintained

eNeuro Accepted Manuscript

122 through homozygous breeding pairs on a C57BL/6 background. In these
123 transgenic mice (nestin-Cre^{ERT2}/AhR$^{f/f}$), tamoxifen treatment suppresses the
124 expression of AhR in the neuroprogenitor cells present at the hippocampal
125 subgranular zone (SGZ). The tamoxifen protocol used in this study was as
126 described before (Cancino et al., 2013). Briefly, both AhR$^{f/f}$ and AhR-icKO mice
127 were administered tamoxifen intraperitoneally in two different rounds. The first
128 round was performed at p30 and the second at p60, each round consisting of a
129 daily injection of tamoxifen (180mg/Kg) in sunflower oil for 5 consecutive days.
130 Behavioural and histological analyses were performed 3 weeks after the last
131 tamoxifen administration. Mice had access to rodent chow and water *ad libitum*
132 in a 12 h light/dark cycle room. This study was approved by the Animal Welfare
133 Committee of the Authors' Institution.
134
135 **BrdU treatment**
136 For quantification of the proportion of proliferating SGZ neural
137 precursors, a total of 4 injections of the cell proliferation marker BrdU (5-bromo-
138 2'-deoxyuridine; 100 mg/kg; Sigma-Aldrich) were administered intraperitoneally
139 every 2h to 4, 8 and 14-weeks-old control and AhR$^{-/-}$ mice. Twenty-four hours
140 after the last administration, mice were sacrificed.
141 For the quantification of the integrated adult newborn neurons
142 (BrdU^{+}/calbindin^{+} cells), 8-weeks-old WT and AhR$^{-/-}$ mice were injected daily
143 with BrdU (100 mg/kg) intraperitoneally for 5 consecutive days, and mice were
144 sacrificed 28 days after the last administration.
145

eNeuro Accepted Manuscript

146 **Histology**

147 For histology and immunohistochemistry studies, mice were perfused
148 transcardially with 0.1M PBS followed by 4% paraformaldehyde (PFA) in 0.1M
149 PBS (pH 7.4). Brains were post-fixed in PFA and transferred to 30% sucrose.
150 For SVZ (from bregma +1.70 mm to bregma 0.02 mm) and dentate gyrus (DG;
151 from bregma -1.46 mm to bregma -2.03 mm), coronal sections (30μm) were cut
152 using a microtome (Leica SM2000R) and stored in cryoprotective solution.
153 Unless indicated otherwise, brain samples from $AhR^{-/-}$ knockout and AhR icKO
154 mice after tamoxifen treatment were analysed at 2 and 3 months of age,
155 respectively.

156 *Immunohistochemistry*: Immunofluorescence was performed on free-
157 floating sections. Briefly, sections were first permeabilized and blocked in
158 0.25% TritonX100 in PBS with 10% normal serum for 1 hour and then,
159 incubated overnight at 4ºC with the following primary antibodies in 0.25% Triton
160 X100 in PBS with 5% normal serum: goat anti-calbindin (neuronal marker;
161 1:500, SantaCruz), goat anti-DCX (doublecortin; neuroblast marker) (1:250,
162 SantaCruz), rabbit anti-Ki67 (nuclear protein specifically expressed in cells
163 undergoing active proliferation; 1:500, Abcam), chicken anti-GFAP (glial
164 fibrillary acidic protein; astrocyte marker; 1:750, Thermo Scientific), mouse anti-
165 nestin-PE (neural stem cell marker; 1:50, BD Biosciences), rabbit anti-AhR
166 (1:200, Enzo Life Sciences) and chicken anti-GFP (1:700, Thermo Scientific).
167 For BrdU staining, free-floating sections were pre-treated with 2 N HCl for 30
168 minutes at 37ºC and, after blocking in 0.25% Triton X100 in PBS with 10%
169 normal serum for 1 hour, incubated overnight at 4ºC with rat monoclonal anti-
170 BrdU (1:200, Abcam) in 0.25% Triton X100 in PBS with 5% normal serum. The

eNeuro Accepted Manuscript

171 secondary antibodies used were donkey Alexa-488 anti-goat (1:500,
172 Invitrogen), donkey Cy3 anti-mouse (1:500, Vector Laboratories), goat anti-rat
173 biotinylated (1:250, Vector Laboratories), streptavidin Alexa-488 conjugate
174 (1:500, Thermo Scientific), goat Alexa-647 anti-chicken (1:500, Thermo
175 Scientific), donkey Cy3 anti-rabbit (1:500, Thermo Scientific) and donkey Alexa-
176 488 anti-chicken (1:500, Thermo Scientific) in 0.25% Triton X100 in PBS with
177 5% normal serum. Controls performed in parallel without primary antibodies
178 showed very low levels of nonspecific staining.

179 *Image processing and quantitative analysis of immunostained sections*:
180 Image acquisition was performed with a laser-scanning confocal imaging
181 system (Zeiss LSM710) and image analysis was accomplished with the
182 ZEN2009 software (Zeiss). Image quantification was performed with ImageJ
183 Software (NIH) and Volocity Software (Improvision). $Ki67^+$, DCX^+, $nestin^+$ and
184 $BrdU^+$ cells were counted in confocal z-stack images. In all cases, quantification
185 was performed using non-stereological methods. Specifically, every 5th section
186 (30 μm, separated 150 μm apart) was selected for a total of 5 representative
187 matched sections per hippocampus (from bregma -1.46mm to bregma -2.06
188 mm) and SVZ (from bregma +1.70 mm to bregma 0.02 mm). Cells were
189 counted manually in frames of 212.55μm x 212.55μm (1024x1024) and data
190 were expressed as the number of cells per 1000 $μm^2$. Since assessment of 5
191 sections may not reflect changes in hippocampal size and extent, quantification
192 data should not be considered in terms of absolute numbers. Although
193 stereological assessment would be more accurate, the fact that cell numbers in
194 $AhR^{-/-}$ mice ranged from being in excess to no differences with age suggests
195 that the methods we have employed are sensitive to major changes that occur

196 with development. Co-localisation of calbindin^{+}/BrdU^{+}, nestin^{+}/BrdU^{+},
197 nestin^{+}/GFAP^{+}, nestin^{+}/GFAP^{+}/BrdU^{+} was confirmed by orthogonal projection of
198 z-stack files.

199 In p60 AhR$^{-/-}$ and p90 AhR-icKO mice and their respective controls,
200 apical dendrite length of DCX^{+} cells was assessed in 5 serial sections (30 μm)
201 from dorsal hippocampus (from bregma -1.46mm to bregma -2.06 mm). Apical
202 dendrite (considered the segment between the soma and the first dendrite
203 ramification) was manually traced in confocal z-stack images taken at 63X and
204 then dendritic length was measured by ImageJ. A total of 20-50 cells per animal
205 from each group were quantified.

206 DCX^{+} dendritic staining was performed in confocal z-stack images taken
207 at 40X. Briefly, rectangular ROIs were generated around neuroblast dendritic
208 arborisation and somas. Total dendritic arborisation (distribution pattern of
209 neuroblast dendrites along granular and molecular layers of the DG) was also
210 subdivided in 2 ROIs for differentiating proximal (GL) and distal (ML) DCX^{+}
211 dendritic staining. Integrated density was quantified in each compartment after
212 background subtraction. Total dendritic arborisation/soma, GL/soma and
213 ML/soma ratios were calculated from these values. This method was internally
214 normalized for immunostaining variability, since immunofluorescence values
215 were always acquired in pairs of dendrites and adjacent somas.

216

217 ***Ex vivo* flow cytometry from SGZ and SVZ-derived NPCs**

218 To quantify the proportion of proliferating SGZ or SVZ neural precursors,
219 mice were injected four times with 100 mg/Kg BrdU intraperitoneally every 2 h
220 and sacrificed 24 h later. Brains were rapidly removed and SVZ and SGZ-

eNeuro Accepted Manuscript

eNeuro Accepted Manuscript

221 derived NPCs of WT and AhR$^{-/-}$ mice were dissected, placed in ice-cold PBS
222 and dissociated into a single cell suspension. Cell suspensions were filtered on
223 40 um nylon mesh strainers and centrifuged at 300g for 10min at room
224 temperature. Next, cells were fixed, permeabilised and stained with anti-BrdU-
225 APC and anti-Nestin-PE according to manufacturer´s instructions (BD
226 Cytofix/Cytoperm Kit, BrdU Flow Kits BD Biosciences). Finally, cells were
227 washed and resuspended in 300 µl FACS Flow (BD Pharmingen); isotype
228 controls (Miltenyi) were run in parallel. Whole suspensions were examined in a
229 FACSCalibur flow cytometer using CellQuest software (BD Pharmingen) and
230 data were analysed using FlowJo software (Tree Star Inc),
231

232 **Golgi-Cox staining**

233 The fresh brain from 8-weeks-old AhR$^{-/-}$ and WT mice without perfusion
234 were used for Golgi-Cox staining with FD Rapid GolgiStain Kit (FD Neuro
235 Technologies, Columbia, MD, USA) according to the user manual. Briefly, the
236 brain was first placed in impregnation solution for 2 weeks followed by 2 days in
237 30% sucrose. Then, brains were cut into 100-µm coronal sections using a
238 vibratome (Leica VT1000s) and stained. Neuronal reconstruction from each
239 animal were randomly drawn at 40X magnification for the different analysis by
240 using the Neurolucida neuron tracing system (Microbrightfield, Colchester, VT).
241 Determination of total dendritic length of branches and Sholl analysis were
242 performed by using the Neuroexplorer software (Microbrightfield, Colchester,
243 VT). Sholl analysis was carried out by counting the number of dendrites that
244 crossed a series of concentric circles at 10 µm intervals from the cell soma. To
245 calculate spine density of Golgi-stained neurons in the DG, a random 10-µm

eNeuro Accepted Manuscript

246 long dendrite segment in the molecular layer was measured (100-200 μm from
247 the soma) and total number of spines was traced. The spine density was
248 determined by dividing the total number of spines by the 10-μm length of the
249 dendritic segment.
250

251 **Retrovirus-mediated labelling and morphological analysis of GFP⁺-**
252 **newborn neurons**

253 New neurons were labelled using a murine Moloney leukemia virus-
254 based retroviral vector (CAG-GFP, a gift from Fred Gage, Salk Institute, La
255 Jolla, CA) (Zhao et al., 2006). Concentrated viral solutions were prepared by
256 transfection of retroviral vectors into Gryphon Eco cells, followed by
257 ultracentrifugation of viral supernatant and concentrated virus solution by ultra-
258 speed centrifugation (average 3 x 10^7 iu/ml). Mice (8-weeks-old) were
259 anesthetized with isoflurane and placed in a stereotaxic frame. Two-μl retrovirus
260 was infused at a rate of 0.2 μl/min into the DG (-2 mm AP, -1.4 mm ML relative
261 to bregma, and 2.4 mm DV from skull) with a 5-μl 32-gauge Hamilton syringe.
262 After the infusion, we allowed 5 extra min to avoid the retrovirus flow during
263 syringe releasing. Twenty-eight days after the viral infusion, mice from all
264 groups were sacrificed for GFP morphological experiments.

265 For morphometric analysis, 50-μm sections were used. A total of 10
266 sections of two series from each animal were used for immunohistochemical
267 detection of GFP-labelled neurons. Eight-ten randomly selected neurons from
268 each group were reconstructed. Confocal 40X stacks of images were obtained
269 and z-projections were analysed to determine total dendritic length and to
270 perform Sholl analysis. All cells were traced using *NeuronJ* plugin for ImageJ

eNeuro Accepted Manuscript

271 software. Sholl analysis was performed in order to determine dendritic
272 complexity using the plugin Sholl Analysis for ImageJ (Ferreira et al., 2014).
273 Primary apical dendrite length was manually traced from the soma until
274 the first dendrite ramification point in randomly selected neurons, and measured
275 by ImageJ.
276 For spine analysis, images of GFP-labelled dendritic processes at the
277 outer molecular layer were acquired at 0.5-μm intervals with a Zeiss LSM710
278 confocal microscope with a plan apochromatic 63X oil lens [numerical aperture
279 (NA), 1.4] and a digital zoom of 3X. The lsm images files were subjected to two
280 iterations of deconvolution with the AutoDeblur program (AutoQuant, Troy, NY).
281 The length of each dendritic segment was measured, and total number of
282 spines in proximal (50-100 μm from the soma) and distal (100-200 μm from the
283 soma) dendritic segments were manually counted. The spine density was
284 determined by dividing the total number of spines by the length of the dendritic
285 segment.
286 Mushroom spines in proximal (50-100 μm from the soma) and distal
287 (100-200 μm from the soma) dendritic segments were identified when the
288 estimated surface area (= $\pi \times D_{major} \times D_{minor}/4$) was ≥ 0.4 μm^2 (Zhao et al.,
289 2014; Zhao et al., 2006). For the quantification, 8-12 dendritic segments from
290 each animal per group were used. Confocal imaging and data quantification
291 were performed blinded to the experimental conditions.
292
293 **Electrophysiology experiments**
294 $AhR^{-/-}$ and WT mice (30- to 45-days-old) were anaesthetized with
295 isoflurane (1.5-2% in a mixture of 80% synthetic air/20% oxygen) and

eNeuro Accepted Manuscript

296 decapitated. The brain was quickly removed and placed in ice-cold artificial CSF
297 (ACSF) containing (in mM): NaCl 124, KCl 2.69, KH_2PO4 1.25, $MgSO_4$ 2,
298 $NaHCO_3$ 26, $CaCl_2$ 2, ascorbic acid 0.4 and glucose 10, continuously bubbled
299 with carbogen (95% O_2 and 5% CO_2; pH 7.3). Sagital hippocampal slices (325-
300 µm thick) were obtained using a Leica VT 1200S vibratome and incubated (≥ 1
301 h) in a holding chamber at room temperature (21-24ºC) in ACSF. Slices were
302 transferred to an immersion recording chamber and superfused at 1mL/min with
303 gassed ACSF including 50 µM picrotoxin to block $GABA_A$ receptors.
304 Experiments were performed at 25°C by using a temperature controller (Warner
305 Instruments). Granule cells from dentate gyrus were visualized under a 40x
306 water immersion objective and a Nomarski condenser combined with infrared
307 microscopy using differential interface contrast (DIC) in an Eclipse FN1 Nikon
308 microscope. Whole-cell electrophysiological recordings from granule cells were
309 performed using patch pipettes (3-4 MΩ resistance) pulled from thick-walled
310 borosilicate glass (1.5 mm outer diameter and 1.1 mm inner diameter) on a P-
311 97 puller (Sutter-Instrument) and filled with the internal solution containing (in
312 mM): K-Gluconate 135, KCl 10, HEPES 10, $MgCl_2$ 1, ATP-Na_2 2 (pH = 7.3
313 adjusted with KOH; osmolality 280-290 mOsm/L). After formation of a whole-cell
314 configuration (-70 mV holding potential), current- or voltage-clamp protocols
315 were applied. For the analysis of the firing pattern and current-voltage
316 relationship, in current-clamp mode, a series of increasing currents (30 pA step,
317 500-ms duration with a 3-s interval) were injected. Evoked EPSCs were
318 recorded from dentate gyrus granule cells (voltage-clamp conditions, -70 mV
319 holding potential) by stimulation of glutamatergic afferents from perforant path
320 using a bipolar theta capillary (2-5 µm tip) filled with ACSF and placed in the

eNeuro Accepted Manuscript

321 molecular layer of dentate gyrus. Stimuli were delivered at 0.33 Hz. Paired
322 Pulse Ratio (PPR) was obtained (2nd EPSC/1st EPSC) by delivering paired
323 pulses (20, 50, 75, 100, 150 and 200-ms interstimulus interval). AMPA/NMDA
324 ratio was obtained (2nd EPSC at +40 mV/1st EPSC at -60 mV holding potential)
325 by delivering paired pulses at 50-ms interstimulus interval. Series and input
326 resistances were monitored throughout the experiment using a -5 mV pulse.
327 Recordings were considered stable when the series and input resistances,
328 resting membrane potential and stimulus artefact duration were not changed >
329 20%. Cells that did not meet these criteria were discarded. The same procedure
330 was carried out for electrophysiology recordings in 50-days-old AhR$^{f/f}$ and AhR-
331 icKO mice (four weeks after 5 tamoxifen injections starting at 21-days-old).
332 Recordings were obtained by a PC-ONE amplifier and signals were fed to a
333 Pentium-based PC through a DigiData1322A interface board. The pCLAMP
334 10.2 software was used for stimulus generation, data display, acquisition,
335 storage and analysis.
336
337 **Behavioural testing**
338 *Contextual fear conditioning.* For mice, contextual fear conditioning
339 occurred in test chambers (31 cm x 24 cm x 21 cm) with shock-grid floors. The
340 front, top and back of the chamber were clear acrylic and the sides were
341 modular aluminium. During training, AhR$^{-/-}$ or AhR-icKO and their respective
342 controls were placed in the chamber and, after 2 min of habituation, they
343 received a mild or a weak conditioning protocol based on 3-foot shocks (0.6
344 mA, 2 s duration, 1 min apart) or 1-foot shock (0.48 mA, 2 s duration),
345 respectively. After conditioning, mice were removed from the chamber 1 min

eNeuro Accepted Manuscript

346 after the last shock. Behaviour was recorded by overhead cameras. Freezing
347 (i.e. absence of movement except for breathing) was measured using
348 automated scoring system for mice.

349 *Barnes maze*. A white circular platform (100-cm diameter, 70 cm above
350 the floor) contained 20 holes equally spaced around its perimeter. Under one of
351 the holes, there was an escape box (17 x 13 x 7 cm) filled with paper bedding.
352 The location of this escape hole was always in the same place for all mice. For
353 avoiding navigation based on olfactory or proximal cues within the maze, the
354 platform was rotated before each trial, and the spatial location of the escape
355 hole remained in a fixed location with respect to the distal room cues. During
356 habituation, mice were allowed 5 min to freely explore the maze, with no escape
357 box present. During training, mice were given 3 trials per day for 6 days. On
358 each trial, the mouse was released in the centre of the maze and allowed for 5
359 min to enter the escape box, where it remained for 30 s. If a mouse failed to find
360 the escape box, it was guided by the experimenter. During probe test, the
361 escape box was removed from the maze, and the mouse was allowed to search
362 for 5 min. Time spent around each hole was recorded. Search paths were
363 recorded by an overhead video camera and tracked using automated
364 *Ethowatcher* software.

365 *Novel object recognition (NOR) and novel object location (NOL)*. Mice
366 were placed in a rectangular arena (30 cm x 20 cm x 30 cm) with clear
367 sidewalls containing two objects (A and B) for 8-min training session and
368 returned to their home cages. The memory tests were performed as described
369 (Nakashiba et al., 2008). Briefly, during the 8-min training phase of object
370 recognition, two identical objects were placed in the arena. For the NOR test,

eNeuro Accepted Manuscript

371 the animal´s memory of one of the original objects was assessed by comparing
372 the amount of time spent exploring a novel object compared with that spent
373 exploring the familiar one during 8 min. For the NOL test, after the training
374 period, the animal´s memory of one of the original objects was assessed by
375 comparing the amount of time spent exploring the new located object with that
376 spent exploring the original located one during 8 min. In both tests, the time
377 spent exploring each object was expressed as a percentage of exploration time
378 [% Exploration time = $(t_{novel}-t_{familiar})/(t_{novel}+t_{familiar})$]. Behaviour was recorded by
379 overhead cameras and videos analyses were performed by a blinded
380 experimenter.

381 *Y-maze*. The Y-maze was made of three solid white arms of equal size
382 (35-cm long and 5-cm wide with 10-cm high walls) joined in a Y-configuration.
383 The maze was cleaned with 70% ethanol between animals to eliminate traces
384 of odour. For working memory, during habituation phase mice were placed
385 where the arms joined and allowed to freely explore the three arms for 6 min.
386 Arm entry was defined as having forelimbs inside an arm. The number of
387 entries was recorded in order to calculate the alternation percentage (defined as
388 a set of consecutive arm entries), which was calculated by dividing the number
389 of triads by the number of possible alternations multiplied by 100. For spatial
390 memory, during training phase mice were allowed to explore two of the three
391 arms for a total of 6 min while the third arm was blocked. Six hours later mice
392 were placed back in the maze for 6 min with all arms open, and the number of
393 entries in each arm was recorded. Behaviour was recorded by overhead
394 cameras and videos analyses were performed by a blinded experimenter.

eNeuro Accepted Manuscript

395 In order to avoid a possible interference due to the manipulation, training
396 and testing on the histological studies, we used different mouse cohorts for
397 each set of experiments. Specifically, two separate mouse cohorts were used
398 for both contextual fear conditioning and Barnes maze. For the rest of the
399 behavioural testing, we used two different groups of mice. One group was first
400 trained in NOR and one week later in NOL and, in the other one, mice were first
401 tested on Y-maze and one week later in NOL.
402
403 **Statistical analysis**
404 Results are expressed as mean ± SEM. Sample sizes for each
405 experiment are indicated in the figure legends. In most experiments, sample
406 size was estimated based on previous extensive experience with similar
407 approaches. For specific experiments, we performed power analysis to
408 adequate sample size with data from pilot studies (usually data from 3
409 animals/group) by calculating power analysis (http://www.biomath.info) with a
410 significance level of 5% and ≥ 80% of power. Cohen's d was used to calculate
411 effect size, with observed strong size effects (d values) ≥ 0.8 (Cohen, 1988).
412 Statistical significance was determined by use of a non-parametric, 2-tailed
413 Mann-Whitney *t* test; or a nonparametric, 2-way ANOVA followed by Bonferroni
414 post hoc testing. Values of $p<0.05$ were considered statistically significant. All
415 statistical analyses were performed with Prism version 5.0 (GraphPad Software,
416 Inc).
417
418 **RESULTS**
419 **Hippocampus-dependent memory is impaired in AhR$^{-/-}$ mice**

eNeuro Accepted Manuscript

420 In order to test whether AhR plays a role in hippocampus-dependent
421 memory, 8-weeks-old $AhR^{-/-}$ mice and their WT littermates were subjected to a
422 battery of hippocampus-dependent tests. First, mice were trained in contextual
423 fear conditioning (CFC), an associative learning which involves the
424 hippocampus (Anagnostaras et al., 2001). No differences were found between
425 WT and $AhR^{-/-}$ mice in response to the foot shock (data not shown), indicating
426 similar levels of nociception in both genotypes. During the retrieval, $AhR^{-/-}$ mice
427 displayed a reduced freezing response in both 1h- and 24h-tests ($p<0.05$;
428 Figure. 1A), and a decreased percentage of activity suppression (88.94 ± 3.52
429 vs. 61.50 ± 9.89% activity suppression in $AhR^{+/+}$ vs. $AhR^{-/-}$ mice, respectively,
430 $p<0.05$) compared with the control group, indicating a reduced fear memory in
431 $AhR^{-/-}$ mice, in agreement with previous evidence (Latchney et al., 2013). To
432 confirm our results we checked other types of hippocampus-dependent memory
433 such as the novel object recognition (NOR) task that relies on mouse natural
434 exploratory behaviour (Ennaceur and Delacour, 1988). During the training
435 session (two similar objects), no preference was detected for one object over
436 the other in both genotypes (data not shown); however, during the test session,
437 whereas WT mice presented a preferential exploration toward the new object,
438 $AhR^{-/-}$ mice exhibited impaired NOR performance with a lack of net preference
439 for any of the objects (significant interaction between genotype and novel/old
440 object recognition two-way ANOVA; $F_{(1, 18)}=7.46$; $p=0.0137$; Fig. 1B). In
441 addition, we checked whether spatial memory was also altered in $AhR^{-/-}$ mice.
442 First, mice were subjected to a novel object location task (NOL) (Antunes and
443 Biala, 2012), in which WT mice spent more time investigating the new location
444 whereas, on the contrary, $AhR^{-/-}$ mice explored similarly both locations

445 (significant interaction between genotype and novel/familiar location exploration
446 two-way ANOVA; $F_{(1, 42)}=7.93$; $p=0.0074$; Fig. 1C). The impairment in spatial
447 memory shown by $AhR^{-/-}$ mice was corroborated by using the Y-maze and the
448 Barnes maze. In the first one, no differences were observed in spatial working
449 memory calculated either as percentage of spontaneous alternation (SAP) or as
450 arm entries (% SAP: 63.14 ± 2.40 vs. 55.21 ± 2.81 in $AhR^{+/+}$ vs. $AhR^{-/-}$ mice,
451 respectively, $p>0.05$; arm entries: 26.43 ± 2.86 vs. 24.40 ± 5.39 in $AhR^{+/+}$ vs.
452 $AhR^{-/-}$ mice, respectively $p>0.05$; Fig. 1D) but, relative to WT, $AhR^{-/-}$ mice did not
453 show any preference toward the novel arm (two-way ANOVA; $F_{(2, 27)}=3.84$;
454 $p=0.0342$; Fig. 1D). In the Barnes maze (Fig. 1E), AhR KO mice and their WT
455 littermates spent similar time to find the escape box during all training sessions.
456 However, during the 24h-probe test, whereas WT animals spent most part of
457 the time in the target hole, $AhR^{-/-}$ ones did not (two-way ANOVA; $F_{(1.8, 19)}=260$;
458 $p=0.0204$; Fig. 1G). These results indicate impairment of the spatial memory
459 and support that AhR is required for a proper function of hippocampus-
460 dependent memory.
461

462 **Hippocampus-dependent memory deficits in $AhR^{-/-}$ mice are independent**
463 **of the levels of hippocampal neurogenesis**

464 AhR-dependent impairment of hippocampal function in $AhR^{-/-}$ mice could
465 be due to a decrease in the levels of hippocampal neurogenesis, consistent with
466 previous studies of AhR in this setting performed at 3 months (P90) (Latchney
467 et al., 2013). Interestingly, when animals were pulsed at different ages (p30,
468 p60 and p100) with 4 consecutive BrdU injections (see Methods for details) at
469 2h-intervals and euthanized 24h after the last injection, higher levels of

eNeuro Accepted Manuscript

eNeuro Accepted Manuscript

470 proliferation at p30 and p60 but not at p100 were detected in AhR$^{-/-}$ mice vs
471 their WT littermates (Fig. 2A). The results at p30 and p100 were confirmed
472 when we quantified the number of cells in cell cycle (using Ki67, marker of cells
473 in active proliferation) in the SGZ of WT and AhR$^{-/-}$ mice (Fig. 2B-C). Since
474 memory studies had been performed at p60, deficits in proliferation are
475 therefore unlikely to account for hippocampal deficits in AhR KO mice, though
476 they may contribute to those reported previously at 3 months (P90; Latchney et
477 al., 2013). Further confirming this finding, at p60, AhR$^{-/-}$ mice displayed around
478 60% increase in the number of proliferative nestin^{+} precursors (nestin^{+}/BrdU^{+}) in
479 the DG when compared with WT ones, determined by flow cytometry 24h after
480 BrdU administration ($p<0.05$; Fig. 2D-F). Furthermore, these data were
481 corroborated by analysing both type-1 (nestin^{+}/GFAP^{+}) and type-2
482 (nestin^{+}/GFAP^{-}) neural progenitor cells, as well as their respective proliferation
483 rates at p30 and p100 (Fig. 2G-L). At p30, AhR$^{-/-}$ mice presented significantly
484 higher levels of type-1 and -2 NPCs and its proliferative population than the
485 control group but, even though at p100 the population of type-1 cells was similar
486 ($p>0.05$; Fig. 2G), type-2 and both type-1 and type-2 proliferative AhR$^{-/-}$ NPCs
487 populations were dramatically decreased ($p<0.05$, Fig. 2G-J) compared to WT
488 populations.

489 To check whether the increase in SGZ proliferation induced by AhR
490 absence was accompanied with a parallel increase in the number of adult
491 newborn neurons, we first studied immunostaining of DCX, a marker of
492 neuroblasts which is transiently expressed in new neurons. Supporting our
493 previous data, p60 AhR$^{-/-}$ mice displayed higher numbers of DCX^{+} cells,
494 indicating immature neurons ($p<0.05$, Fig. 2M). In addition, we administered

eNeuro Accepted Manuscript

495 BrdU during 5 days and, 28d later, we analysed the number of newborn mature
496 neurons as $BrdU^{+}$ cells expressing the mature neuronal marker calbindin.
497 Quantifications demonstrated that $AhR^{-/-}$ mice present a significant increase in
498 the number of total $BrdU^{+}$ cells and of double $BrdU^{+}$/$calbindin^{+}$ cells ($p<0.05$;
499 Fig. 2O), denoting that AhR absence leads to an increase in the number of
500 newly generated neurons. Furthermore, a comparable percentage of
501 $BrdU^{+}$/$calbindin^{+}$ cells was estimated for both groups (56% $AhR^{-/-}$ vs. 55% WT),
502 suggesting that AhR deletion does not modify differentiation rate.

503 Similarly, neurogenesis enhancement attributable to the absence of AhR,
504 determined by quantification of $BrdU^{+}$/$nestin^{+}$ cells (4862 ± 561 vs. 8072 ± 851
505 cells in $AhR^{+/+}$ vs. $AhR^{-/-}$ mice, respectively, $p<0.05$, n=6), $Ki67^{+}$ cells (276 ± 29
506 vs. 430 ± 23 cells in $AhR^{+/+}$ vs. $AhR^{-/-}$ mice, respectively, $p<0.05$, n=5) and
507 DCX^{+} volume (3707 ± 364 vs 6291 ± 545 μm^3 in $AhR^{+/+}$ vs. $AhR^{-/-}$ p60 mice,
508 respectively, $p<0.05$, n=5), was also observed in the other adult neurogenic
509 niche, the subventricular zone (SVZ). Thus, a common shared mechanism
510 underlying the actions of AhR in both neurogenic niches can be suggested.

511 Therefore, despite previously suggested role of AhR (Latchney et al.,
512 2013), our data indicate that, at p30 and at p60, the absence of AhR enhances
513 or does not affect hippocampal neurogenesis, thus discarding that
514 hippocampus-dependent deficits observed in $AhR^{-/-}$ mice at p60 are due to
515 decreased levels of adult neurogenesis.

516

517 **Absence of AhR is associated to aberrant morphology of hippocampal**
518 **granule cells**

eNeuro Accepted Manuscript

519 A high rate of adult hippocampal neurogenesis has been previously
520 demonstrated to correlate positively with increased learning and memory ability
521 (Kempermann et al., 1997; van Praag et al., 2002). Given that AhR$^{-/-}$ mice
522 exhibit impaired memory when hippocampal neurogenesis is still enhanced and
523 considering the high AhR mRNA expression in the DG granular layer (Kimura
524 and Tohyama, 2017) and the reported role of AhR orthologues in the control of
525 neuronal growth and dendritic arborisation in invertebrates (Crews and
526 Brenman, 2006; Kim et al., 2006; Qin and Powell-Coffman, 2004; Smith et al.,
527 2013), we hypothesised that defects observed when AhR is deleted could be
528 due to variations in the morphology of granule neurons and its subsequent
529 functional activity. Therefore, we examined granule neuronal morphology in
530 hippocampi of WT and AhR$^{-/-}$ p60 mice. First, dendritic branching of DG granule
531 neurons was quantified by Sholl analysis of Golgi-Cox stained sections (Fig. 3A-
532 C). Relative to WT, AhR$^{-/-}$ mice displayed a higher number of dendritic branches
533 close to the soma (40-70 µm from soma; $p<0.05$; Fig. 3A), increased total
534 dendritic length ($p<0.05$; Fig. 3B), and a larger number of dendritic spines
535 ($p<0.05$; Fig. 3C), supporting our hypothesis that the absence of AhR is
536 associated to an altered dendritic structure of granule neurons.

537 Interestingly, similar changes were found in immature neurons (DCX^{+}
538 neuroblasts) in WT and AhR$^{-/-}$ p60 mice, indicating that AhR effects on granule
539 neuronal morphology seem to be also apparent in adult-born granule neurons.
540 Interestingly, quantification of DCX^{+} labelling distribution between total
541 (GL+ML), granular (GL) and molecular layers (ML) revealed significant
542 differences in the arborisation pattern of both genotypes: compared with WT
543 subjects, AhR$^{-/-}$ mice showed increased DCX^{+} staining in GL while no

eNeuro Accepted Manuscript

544 differences were found in the ML ($p<0.05$; Fig. 3D). In addition, immature AhR
545 KO cells also presented a significant reduction in the apical dendrite length
546 ($p<0.05$; Fig. 3E). To confirm that the absence of AhR affects the morphology of
547 adult newborn neurons, high titres of CAG-GFP retrovirus were delivered into
548 the hilar region of WT and $AhR^{-/-}$ KO p60 mice to selectively target proliferating
549 neuronal progenitors *in vivo* (Zhao et al., 2006). Twenty-eight days post-
550 infection, Sholl analysis of GFP newborn neurons in the DG showed an
551 increased dendritic branching in the proximal segment close to the soma of
552 $AhR^{-/-}$ neurons compared to those of WT (50-150 μm from the soma; $p<0.05$;
553 Fig. 3I). While total dendritic length was significantly greater in $AhR^{-/-}/GFP^{+}$
554 neurons ($p<0.05$; Fig. 3J) indicating a higher pattern of branching, the apical
555 dendrite length was shorter than in control/GFP^{+} cells ($p<0.05$; Fig. 3K). Taking
556 all these results together, it can be concluded that the absence of AhR
557 promotes retraction of the apical dendrite and altered branching of the dendritic
558 tree. The aberrant morphology of granular neurons was additionally supported
559 by the finding of a higher dendritic spine density in $AhR^{-/-}/GFP^{+}$ neurons
560 compared to those of WT mice in both, proximal and distal segments of
561 dendritic branches in the molecular layer ($p<0.05$; Fig. 3L). Despite this, the
562 number of mushroom spines in both segments, typically more abundant in
563 mature neurons (Zhao et al., 2006), was significantly lower in $AhR^{-/-}/GFP^{+}$ cells
564 than in $AhR^{+/+}/GFP^{+}$ neurons along the dendrites in the molecular layer ($p<0.05$;
565 Fig. 3M), thus suggesting a more immature phenotype in the absence of AhR.
566
567 **The lack of AhR alters granule cells intrinsic excitability, synapses**
568 **maturation and the correct function of the hippocampus**

eNeuro Accepted Manuscript

569 Morphological changes resulting from AhR ablation can lead to
570 alterations of the hippocampal physiological properties. This possibility was
571 investigated by performing electrophysiological analysis of granule cells in acute
572 slices from $AhR^{-/-}$ and control mice (Fig. 4A). Previously, the absence of
573 significant differences between groups in resting membrane potential and
574 membrane resistance was verified (Fig. 4B-C). Then, the ability of $AhR^{-/-}$
575 granule cells to fire repetitive action potentials, a hallmark of neuronal
576 maturation (Deng et al., 2010), was assessed. Under the whole-cell current-
577 clamp, $AhR^{-/-}$ granule cells showed an increased firing rate in response to a
578 depolarizing current injection (40-190 pA; $p<0.05$; Fig. 4D-E), consistent with
579 immature neuronal excitability (Dieni et al., 2016). It is known that the ratio of
580 active/silent synapses is changing over neuron maturation as a result of
581 changes in the content of glutamate AMPA receptors (AMPARs) (Carlisle and
582 Kennedy, 2005; Chater and Goda, 2014; Paoletti et al., 2013; Tada and Sheng,
583 2006). In order to assess functional AMPAR content, we quantified the
584 AMPAR/NMDAR ratio by comparing AMPA excitatory postsynaptic currents
585 (EPSCs) at -70mV and glutamate NMDA receptors (NMDARs) EPSCs at
586 +40mV in WT and $AhR^{-/-}$ granule cells. We found a significantly lower
587 AMPAR/NMDAR ratio in $AhR^{-/-}$ granule cells, indicating a lower proportion of
588 AMPAR to NMDAR on their granule cell dendrites ($p<0.05$; Fig. 4F-G), thus
589 suggesting that $AhR^{-/-}$ granule cells have a more immature phenotype than
590 those from WT. Finally, we studied the pair-pulse ratio (PPR) as a
591 hippocampus-dependent function measurement for integration of inputs coming
592 from the entorhinal cortex to the hippocampal granule cells. The PPR
593 (EPSC2/EPSC1) was significantly higher in $AhR^{-/-}$ KO compared with control

eNeuro Accepted Manuscript

594 mice ($p<0.05$; Fig. 4H), indicating that the initial probability of release is lower in
595 AhR$^{-/-}$ KO mice.
596
597 **Absence of AhR in neural progenitor cells is enough to promote**
598 **hippocampal deficits**
599 In order to check the specific role of AhR in adult-born granule neurons,
600 we used a transgenic strategy to conditionally delete AhR from neural
601 progenitor cells in adult mice (AhR-icKO mice; Fig. 5A). For such purpose we
602 crossed mice expressing tamoxifen (TAM)-inducible Cre-recombinase driven by
603 a progenitor specific promoter (nestin-Cre^{ERT2} mice) (Imayoshi et al., 2008) with
604 mice in which AhR is floxed (AhR$^{f/f}$) (Walisser et al., 2005). In double mutant
605 offspring from this cross (AhR-icKO), TAM treatment (Fig. 5A, bottom) induced
606 the excision of the exon 2 flanked sequences and the deletion of AhR in neural
607 progenitor cells and their progeny resulted in a marked decrease of AhR
608 expression in the DG determined by immunofluorescence (Fig. 5B).
609 Examination of 3-month-old animals after tamoxifen administration revealed a
610 higher number of DCX^{+} cells in the SGZ of the AhR-icKO mice than in that of
611 control mice ($p<0.05$; Fig. 5C) although not significant differences were found
612 for Ki67^{+} cells (29.28 ± 2.93 vs. 33.47 ± 1.86 in AhR$^{+/+}$ vs. AhR$^{-/-}$ mice,
613 respectively, $p>0.05$). Consistent with these data, AhR-icKO mice treated with
614 TAM presented an increased DCX staining in total (GL+ML) and GL but not in
615 the ML ($p<0.05$; Fig. 5D), similar to AhR$^{-/-}$ mice. In order to study whether
616 morphological alterations present in newborn neurons were affecting cognitive
617 ability, memory tests were carried out. First, we analysed episodic memory in
618 CFC test using a weak fear conditioning protocol based on one-foot shock

eNeuro Accepted Manuscript

619 stimuli in order to detect subtle differences which are not masked by
620 generalisation (Lonsdorf et al., 2017). Remarkably, in agreement with our
621 results in AhR$^{-/-}$ mice, AhR-icKO mice displayed comparable cognitive
622 hippocampal deficits in CFC, showing a reduced freezing response compared
623 to AhR$^{f/f}$ ($p<0.05$; Fig. 5E). Similarly, in the Y-maze test, only AhR$^{f/f}$ mice
624 showed a preference towards the closed arm (significant interaction between
625 genotype and closed arm two-way ANOVA; $F_{(2, 57)}$=5,91; p=0.0047; Fig. 5F).
626 Finally, NOL test revealed that the specific ablation of AhR in adult
627 neuroprogenitor cells in AhR-icKO mice pattern separation skills is altered,
628 showing a worst discrimination efficiency than AhR$^{f/f}$ mice, not demonstrating
629 any kind of preference for the new location (Fig. 5G).
630

631 **Acute conditional deletion of AhR in neuroprogenitor cells is enough to**
632 **alter granule cell intrinsic excitability, synapses maturation and the**
633 **correct function of the hippocampus**

634 To examine whether the functional properties of the aberrant newborn
635 neurons might underlie hippocampus-dependent memory impairments
636 observed in our AhR-icKO, we acutely ablated AhR in adult neuroprogenitor
637 cells by treating p21 AhR$^{f/f}$ and AhR-icKO mice with tamoxifen, and
638 electrophysiological studies were performed 4 weeks after the last tamoxifen
639 administration (Fig. 6A). We did not see any differences between groups in
640 resting potential and membrane resistance (Fig. 6B-C). When we analysed the
641 intrinsic excitability of AhR$^{f/f}$ and AhR-icKO granule neurons measured as the
642 ability to spike action potentials by stimulating them with increased electrical
643 depolarization currents, we found that acute ablation of AhR in adult

eNeuro Accepted Manuscript

644 neuroprogenitor cells led to a significant increase in the intrinsic excitability of
645 AhR-icKO granule neurons ($p<0.05$; Fig. 6D-E), consistently with our previous
646 results in constitutive AhR KO mice. Given the importance of AMPA receptors in
647 maturation and functionality of the synapses, AMPAR and NMDAR-mediated
648 currents were measured in order to explore the ability to integrate and respond
649 to the inputs coming from the entorhinal cortex into the hippocampus by the
650 granule neurons. Confirming our results in $AhR^{-/-}$, AhR-icKO granule neurons
651 displayed a reduction in AMPA/NMDA ratio indicating that the specific absence
652 of AhR in newborn granule neurons impairs a correct dendritic spine maturation
653 ($p<0.05$; Fig. 6F-G). Finally, we studied the PPR in these mice to explore the
654 connectivity between EC and DG. According with our previous results in AhR
655 KO mice, AhR-icKO granule neurons showed significant higher PPR
656 (EPSC2/EPSC1) compared with $AhR^{f/f}$ cells (Fig. 6H), meaning an initial lower
657 neurotransmitter probability of release when AhR is acutely ablate.
658

659 **DISCUSSION**

660 We have investigated the role of the transcription factor AhR in
661 hippocampal function and granule neuronal morphology in adult mice brain. Our
662 data demonstrate that AhR absence is associated to a severe impairment of
663 hippocampal-dependent memory, concomitantly to an increased dendrite
664 arborisation pattern and a decreased dendritic spine maturity of hippocampal
665 granule neurons, as well as to aberrant electrophysiological properties and
666 functions of these cells.

667 AhR (Aryl hydrocarbon Receptor) is a basic helix-loop-helix-PER-ARNT-
668 SIM (bHLH-PAS) transcription factor that mediates the toxic and carcinogenic

eNeuro Accepted Manuscript

669 effects of xenobiotics. Interestingly, AhR is widely expressed in the CNS and, in
670 this context, its physiological and pathological roles are just beginning to be
671 unravelled. Specifically, AhR mRNA is enriched in the dentate gyrus granule
672 cells of the adult hippocampus (Kimura and Tohyama, 2017), a crucial structure
673 for high cognition tasks, such as episodic, spatial learning and memory, which
674 are often disrupted in neurological disorders. AhR is the only PAS member
675 known to be activated by endogenous or exogenous ligands (Boitano et al.,
676 2010; Cuartero et al., 2014; Mandal, 2005; Mimura and Fujii-Kuriyama, 2003;
677 Mimura et al., 1997; Nguyen and Bradfield, 2008). The potential therapeutic
678 implications derived from this fact prompted us to study its role in hippocampal
679 function. Here, we demonstrate that the absence of AhR affects different types
680 of hippocampal-dependent tasks such as episodic (NOR and CFC) and spatial
681 memories (Y-maze, NOL and Barnes maze).

682 Hippocampal newborn neurons have been implicated in the acquisition
683 and recall of hippocampus-dependent memories (Aimone et al., 2014; Anacker
684 and Hen, 2017) and, therefore, adult hippocampal neurogenesis is an essential
685 process for cognitive function (Kempermann et al., 1997; van Praag et al., 1999;
686 van Praag et al., 2002; Zhao et al., 2006). The reduced NPC proliferation in the
687 SGZ in parallel to deficits in fear conditioning memory tests which has been
688 described in 12-weeks old AhR-deficient mice (Latchney et al., 2013) could
689 therefore explain the AhR-dependent impairment of episodic and spatial
690 hippocampus-dependent memory mice that we observe in 2-month old (p60)
691 $AhR^{-/-}$. However, on the contrary, we have found that 2-month old (p60) $AhR^{-/-}$
692 mice display enhanced SGZ neurogenesis, as shown by a higher number of
693 newborn NPCs, neuroblasts and fully integrated mature neurons, thus

eNeuro Accepted Manuscript

694 discarding that hippocampus-dependent memory deficits are due to decreased
695 adult neurogenesis. Indeed, we have found that at both p30 and p60, the
696 absence of AhR increases SGZ NPCs proliferation. However, at p100, the
697 process is reversed, with a decrease in NPCs proliferation, similarly to the
698 reported results at 12-weeks old (Latchney et al., 2013). It is plausible that niche
699 depletion induced by the enhanced NPCs proliferation at earlier times accounts
700 for the decreased proliferation at later times in $AhR^{-/-}$ mice. Several studies have
701 reported an increased proliferative response, so-called compensatory
702 proliferation, that takes place in order to counteract an excess of newborn cell
703 death (rev. in Yamaguchi and Miura, 2015). Although the parallel increase in the
704 number of $BrdU^{+}$/$calbindin^{+}$ cells suggests that this mechanism is not taking
705 place in $AhR^{-/-}$ mice, additional studies assessing precursor apoptosis and
706 survival would be required to define the outcomes of excess proliferation in the
707 absence of AhR.

708 In any case, as discussed above, decreased proliferation is not
709 responsible for hippocampal memory deficits in 2-month old mice, supporting
710 that other mechanisms are involved.

711 AhR is a highly-conserved protein from invertebrates to mammals.
712 Although in mammals AhR has been traditionally known to participate in the
713 xenobiotic metabolism of toxic compounds like dioxins (Barouki et al., 2007;
714 Fernandez-Salguero et al., 1996; Fernandez-Salguero et al., 1997; Fujii-
715 Kuriyama and Kawajiri, 2010; Fujii-Kuriyama and Mimura, 2005), invertebrate
716 AhR orthologues do not have a toxic response to dioxin, neither have dioxin
717 binding capacity, what suggests another ancestral role for this receptor that
718 could have remained throughout the evolution. In fact, previous works in *C.*

eNeuro Accepted Manuscript

719 *elegans* (Huang et al., 2004; Qin and Powell-Coffman, 2004; Smith et al., 2013)
720 and *Drosophila* (Crews and Brenman, 2006; Kim et al., 2006) identified AhR
721 orthologues as regulators of dendrite branching in different types of neurons.
722 More recently, in mammals, AhR activation has been reported to disrupt
723 migration and dendritic growth of olfactory interneurons and hippocampal CA1
724 neurons, respectively, in the mouse brain (Kimura et al., 2016; Kimura et al.,
725 2017). However, the specific role of AhR in dendrite morphology and functional
726 activity of DG granule neurons in the adult murine brain is not known. Our
727 studies using Golgi-Cox staining or doublecortin immunofluorescence show
728 altered dendritic structure of granule neurons in the absence of AhR. GFP
729 labelling confirmed that AhR absence affects the morphology of adult newborn
730 neurons, an effect that is likely contributing to the memory deficits exhibited by
731 these mice. $AhR^{-/-}$ newborn neurons show an altered morphology characterised
732 by a shorter apical dendrite and a profuse dendritic branching close to the
733 soma. Since ectopic migration was not observed, the shortening of the apical
734 dendrite in $AhR^{-/-}$ cannot be ascribed to an ectopic pattern of migration in the
735 GL. All these changes could affect the synaptic partners of these neurons, with
736 detrimental consequences for hippocampal-dependent behaviour, and suggest
737 that modifications of AhR function might underlie some pathological situations
738 inducing aberrant granule neuronal morphology.

739 Regarding the morphology of dendritic spines, whereas filopodia and
740 stubby spines are often associated with immature neurons, thin and mushroom
741 spines are more abundant in mature neurons (Carlisle and Kennedy, 2005;
742 Spruston and Johnston, 2008; Zhao et al., 2006). Of note, GFP labelling
743 revealed that $AhR^{-/-}$ granule neurons displayed a higher spine density but a

eNeuro Accepted Manuscript

744 much lower abundance of mature mushroom spines. Thus, reduced dendritic
745 mushroom spine density would further alter excitatory inputs and the number of
746 synaptic inputs and integration (Spruston and Johnston, 2008).

747 Consistently, AhR loss-of-function was associated to an increased
748 intrinsic excitability which could suggest a more immature phenotype (Dieni et
749 al., 2016; Lopez-Rojas and Kreutz, 2016). Previous studies have reported that
750 neuronal membrane resistance as well action potential firing rate decrease
751 along neuronal maturation (Mongiat et al., 2009; Dieni et al., 2016), resulting in
752 an adequate integration of the inputs coming from the entorhinal cortex. These
753 changes are critical factors that contribute to learning and memory in the
754 hippocampus. Our results suggest that AhR could be necessary for this
755 electrophysiological change. We also found a lower AMPAR/NMDAR ratio in
756 granule neurons from $AhR^{-/-}$ mice, probably indicating a selective depression in
757 AMPAR synaptic responses. During physiological granule cell maturation, there
758 is an increase in the number of mature dendritic spines due to a progressive
759 incorporation of AMPARs into the synaptic sites (Bassani et al., 2013). As
760 commented above, AhR deficiency was linked to a higher proportion of
761 immature spines albeit an increased spine density in mature granule cells. Our
762 results support the idea that AhR is necessary for this maturation, very likely by
763 modulating the levels of AMPAR and NMDAR in the dendritic spines. In
764 addition, the PPR (EPSC2/EPSC1) was significantly higher in $AhR^{-/-}$
765 hippocampal slices compared with those from wild-type mice, strongly
766 suggesting that the initial probability of neurotransmitter release in the terminals
767 coming from the entorhinal cortex to the dentate gyrus is reduced in $AhR^{-/-}$ mice
768 (Fioravante and Regehr, 2011). This could suggest an immature phenotype of

eNeuro Accepted Manuscript

769 granule cell dendritic spines that affects synapses in a retrograde fashion, by
770 altering neurotransmitter release from perforant pathway terminals.

771 In contrast with our results, increased rates of neurogenesis and/or high
772 excitability on immature newborn granule cells are two features that have been
773 associated to the role of these cells in learning and memory (Lopez-Rojas and
774 Kreutz, 2016). However, several pieces of evidence in the literature also
775 support that increased neurogenesis may not always result in improved
776 function. For instance, manipulations that increase neurogenesis may have
777 positive effects on anterograde memories but not in retrograde memories
778 (Akers et al., 2014; Frankland et al., 2013). In agreement with our results,
779 pathological situations that impair hippocampal function such as epilepsy (Cho
780 et al., 2015; Zhao et al., 2008) or stroke (Niv et al., 2012; Woitke et al., 2017)
781 trigger an augmented hippocampal neurogenic response which is accompanied
782 by aberrant features of newborn neurons. Of note, these aberrant neurons show
783 a retraction in apical dendrite and an increased aberrant dendrite branching, a
784 phenotype which is considered an immature feature (Woitke et al., 2017) and
785 clearly resembles the one that we have observed in $AhR^{-/-}$ mice. This altered
786 dendritic morphology may, on its turn, underlie the “immature”
787 electrophysiological features described. As commented above, an interesting
788 possibility suggested by our study is that AhR controls dendritic spine formation
789 and maturation, very likely by regulation of the expression and/or the post-
790 translational trafficking of the AMPA receptor, a hypothesis that remains to be
791 studied. A sustained immature status due to the lack of proper dendritic
792 maturation could trigger, as compensatory mechanisms, an intrinsic
793 hyperexcitability and a subsequent lower initial probability of release, that will

eNeuro Accepted Manuscript

794 translate into an increased PPR. Although the underlying mechanisms are likely
795 to differ depending on each pathophysiological circumstance, it has been
796 described that animal paradigms of Alzheimer's disease (AD) show aberrant
797 increases in network excitability in the dentate gyrus hippocampus that may
798 contribute to the neurological deficits shown by these models (Frazzini et al.,
799 2016; Hazra et al., 2013; Palop et al., 2007).

800 To further confirm the role of AhR in hippocampus-dependent memory
801 through the modulation of neurogenesis and granule neurons maturation and
802 activity, we analysed those mechanisms in our specific neuroprogenitors AhR-
803 ablated mice. Of note, we evaluated SGZ NPCs proliferation using animals with
804 specific AhR deletion in nestin-expressing cells. Our data showing higher
805 numbers of immature neurons in the SGZ of AhR icKO mice, and altered
806 dendritic arborisation and electrophysiological properties, similar to those of
807 $AhR^{-/-}$ mice confirm our previous data and allow us to discard indirect effects
808 arising from the total lack of AhR in $AhR^{-/-}$ mice. Besides, similar cognitive
809 impairment was observed after the specific deletion of AhR in neuroprogenitor
810 cells. First, by using a weak protocol in the CFC test, our data showed that the
811 absence of AhR in newborn neurons is enough to disturb episodic memory.
812 Furthermore, similar memory impairment was observed in AhR-icKO mice when
813 they were tested on the Y-maze, NOR and NOL tests, supporting that alteration
814 of the AhR pathway in newborn granule cells, or even changes in the availability
815 of endogenous or exogenous AhR activators, not only may affect their
816 morphological properties, but also could have detrimental repercussions in the
817 function of the hippocampus.

eNeuro Accepted Manuscript

818 As several other members of the bHLH superfamily and consistent with
819 its dynamic pattern expression in the embryonic and postnatal mouse brain at
820 different time points (Kimura & Tohyama, 2017), brain AhR is likely to play both
821 time- and region-specific functions. In agreement with this, it has been shown
822 that AhR activity regulates cerebellar granule neuron number and
823 differentiation, possibly by coordinating granule neuron precursor
824 developmental transition (Dever et al., 2016). Although with different features,
825 our longitudinal study illustrates how hippocampal neurogenesis varies along
826 time from p30 to p100, strongly supporting a role of AhR in the control of
827 proliferation and pool maintenance of adult-hippocampal neural stem cells in an
828 age-dependent way.

829 In addition, several studies report the involvement of AhR in the migration
830 and dendritogenesis of olfactory interneurons and of cortical piramidal neurons
831 during development (Kimura et al., 2016, 2017), as well as in neuronal
832 differentiation in adult mice (Dever et al., 2016). In line with these results, in the
833 present study our data demonstrate the role of AhR as a key modulator of
834 newborn hippocampal granule neuron morphology, including dendritic spine
835 growth and maturation, which are essential for hippocampal function, thus
836 supporting AhR as a main player in neuronal maturation/differentiation. Hence,
837 our study expands the biological implications of AhR receptor in such a relevant
838 function showing that AhR plays time-specific functions in the regulation of
839 neurogenesis and granule neuron maturation in hippocampus. Interestingly,
840 several studies have demonstrated that dioxin exposure interferes with
841 developmental neurogenesis (Latchney et al., 2013; Williamson et al., 2005) so

842 abnormal modulation of AhR by ligands such as environmental pollutants
843 throughout life might lead to hippocampus-related dysfunctions.

844 Summing up, deletion of AhR induces a severe impairment of
845 hippocampal-dependent memory, concomitantly to a high dendrite arborisation
846 pattern in newborn hippocampal neurons, increased density of dendritic spines
847 but a reduction in mature mushroom spines, which drive a phenotype showing
848 aberrant electrophysiological properties and function of these cells. Our study
849 provides evidence indicating that AhR is a regulator of dendrite arborisation and
850 functional activity of adult hippocampal newborn neurons and showing its critical
851 role for learning and memory function. An additional novel line of research
852 opened by our study is the possible implication of AhR, as a new potent
853 druggable target, in disorders in which cognitive deficits are accompanied by
854 hippocampal morphological alterations, such as epilepsy, schizophrenia or
855 stroke.
856

eNeuro Accepted Manuscript

eNeuro Accepted Manuscript

857 **REFERENCES**

858 Aimone, J.B., Li, Y., Lee, S.W., Clemenson, G.D., Deng, W., and Gage, F.H.
859 (2014). Regulation and function of adult neurogenesis: from genes to cognition.
860 Physiol Rev 94, 991-1026.
861 Akers, K.G., Martinez-Canabal, A., Restivo, L., Yiu, A.P., De Cristofaro, A.,
862 Hsiang, H.L., Wheeler, A.L., Guskjolen, A., Niibori, Y., Shoji, H., *et al.* (2014).
863 Hippocampal neurogenesis regulates forgetting during adulthood and infancy.
864 Science 344, 598-602.
865 Altman, J., and Das, G.D. (1965). Autoradiographic and histological evidence of
866 postnatal hippocampal neurogenesis in rats. J Comp Neurol 124, 319-335.
867 Anacker, C., and Hen, R. (2017). Adult hippocampal neurogenesis and
868 cognitive flexibility - linking memory and mood. Nat Rev Neurosci 18, 335-346.
869 Anagnostaras, S.G., Gale, G.D., and Fanselow, M.S. (2001). Hippocampus and
870 contextual fear conditioning: recent controversies and advances. Hippocampus
871 11, 8-17.
872 Antunes, M., and Biala, G. (2012). The novel object recognition memory:
873 neurobiology, test procedure, and its modifications. Cogn Process 13, 93-110.
874 Barouki, R., Coumoul, X., and Fernandez-Salguero, P.M. (2007). The aryl
875 hydrocarbon receptor, more than a xenobiotic-interacting protein. FEBS Lett
876 581, 3608-3615.
877 Bassani, S., Folci, A., Zapata, J., and Passafaro, M. (2013). AMPAR trafficking
878 in synapse maturation and plasticity. Cell Mol Life Sci 70, 4411-4430.
879 Boitano, A.E., Wang, J., Romeo, R., Bouchez, L.C., Parker, A.E., Sutton, S.E.,
880 Walker, J.R., Flaveny, C.A., Perdew, G.H., Denison, M.S., *et al.* (2010). Aryl

eNeuro Accepted Manuscript

881 hydrocarbon receptor antagonists promote the expansion of human
882 hematopoietic stem cells. Science 329, 1345-1348.
883 Carlisle, H.J., and Kennedy, M.B. (2005). Spine architecture and synaptic
884 plasticity. Trends Neurosci 28, 182-187.
885 Chater, T.E., and Goda, Y. (2014). The role of AMPA receptors in postsynaptic
886 mechanisms of synaptic plasticity. Front Cell Neurosci 8, 401.
887 Cho, K.O., Lybrand, Z.R., Ito, N., Brulet, R., Tafacory, F., Zhang, L., Good, L.,
888 Ure, K., Kernie, S.G., Birnbaum, S.G., *et al.* (2015). Aberrant hippocampal
889 neurogenesis contributes to epilepsy and associated cognitive decline. Nat
890 Commun 6, 6606.
891 Crews, S.T., and Brenman, J.E. (2006). Spineless provides a little backbone for
892 dendritic morphogenesis. Genes Dev 20, 2773-2778.
893 Cuartero, M.I., Ballesteros, I., de la Parra, J., Harkin, A.L., Abautret-Daly, A.,
894 Sherwin, E., Fernández-Salguero, P., Corbí, A.L., Lizasoain, I., and Moro, M.A.
895 (2014). L-kynurenine/aryl hydrocarbon receptor pathway mediates brain
896 damage after experimental stroke. Circulation 130, 2040-2051.
897 Deng, W., Aimone, J.B., and Gage, F.H. (2010). New neurons and new
898 memories: how does adult hippocampal neurogenesis affect learning and
899 memory? Nat Rev Neurosci 11, 339-350.
900 Dever, D.P., Adham, Z.O., Thompson, B., Genestine, M., Cherry, J.,
901 Olschowka, J.A., DiCicco-Bloom, E., and Opanashuk, L.A. (2016). Aryl
902 hydrocarbon receptor deletion in cerebellar granule neuron precursors impairs
903 neurogenesis. Dev Neurobiol 76, 533-550.

eNeuro Accepted Manuscript

904 Dieni, C.V., Panichi, R., Aimone, J.B., Kuo, C.T., Wadiche, J.I., and Overstreet-
905 Wadiche, L. (2016). Low excitatory innervation balances high intrinsic
906 excitability of immature dentate neurons. Nat Commun 7, 11313.
907 Ennaceur, A., and Delacour, J. (1988). A new one-trial test for neurobiological
908 studies of memory in rats. 1: Behavioral data. Behav Brain Res 31, 47-59.
909 Fernandez-Salguero, P., Pineau, T., Hilbert, D.M., McPhail, T., Lee, S.S.,
910 Kimura, S., Nebert, D.W., Rudikoff, S., Ward, J.M., and Gonzalez, F.J. (1995).
911 Immune system impairment and hepatic fibrosis in mice lacking the dioxin-
912 binding Ah receptor. Science 268, 722-726.
913 Fernandez-Salguero, P.M., Hilbert, D.M., Rudikoff, S., Ward, J.M., and
914 Gonzalez, F.J. (1996). Aryl-hydrocarbon receptor-deficient mice are resistant to
915 2,3,7,8-tetrachlorodibenzo-p-dioxin-induced toxicity. Toxicol Appl Pharmacol
916 140, 173-179.
917 Fernandez-Salguero, P.M., Ward, J.M., Sundberg, J.P., and Gonzalez, F.J.
918 (1997). Lesions of aryl-hydrocarbon receptor-deficient mice. Vet Pathol 34, 605-
919 614.
920 Ferreira, T.A., Blackman, A.V., Oyrer, J., Jayabal, S., Chung, A.J., Watt, A.J.,
921 Sjöström, P.J., and van Meyel, D.J. (2014). Neuronal morphometry directly from
922 bitmap images. Nat Methods 11, 982-984.
923 Fioravante, D., and Regehr, W.G. (2011). Short-term forms of presynaptic
924 plasticity. Curr Opin Neurobiol 21, 269-274.
925 Frankland, P.W., Köhler, S., and Josselyn, S.A. (2013). Hippocampal
926 neurogenesis and forgetting. Trends Neurosci 36, 497-503.
927 Frazzini, V., Guarnieri, S., Bomba, M., Navarra, R., Morabito, C., Mariggiò,
928 M.A., and Sensi, S.L. (2016). Altered Kv2.1 functioning promotes increased

eNeuro Accepted Manuscript

929 excitability in hippocampal neurons of an Alzheimer's disease mouse model.
930 Cell Death Dis 7, e2100.
931 Fujii-Kuriyama, Y., and Kawajiri, K. (2010). Molecular mechanisms of the
932 physiological functions of the aryl hydrocarbon (dioxin) receptor, a
933 multifunctional regulator that senses and responds to environmental stimuli.
934 Proc Jpn Acad Ser B Phys Biol Sci 86, 40-53.
935 Fujii-Kuriyama, Y., and Mimura, J. (2005). Molecular mechanisms of AhR
936 functions in the regulation of cytochrome P450 genes. Biochem Biophys Res
937 Commun 338, 311-317.
938 Hazra, A., Gu, F., Aulakh, A., Berridge, C., Eriksen, J.L., and Ziburkus, J.
939 (2013). Inhibitory neuron and hippocampal circuit dysfunction in an aged mouse
940 model of Alzheimer's disease. PLoS One 8, e64318.
941 Huang, X., Powell-Coffman, J.A., and Jin, Y. (2004). The AHR-1 aryl
942 hydrocarbon receptor and its co-factor the AHA-1 aryl hydrocarbon receptor
943 nuclear translocator specify GABAergic neuron cell fate in C. elegans.
944 Development 131, 819-828.
945 Imayoshi, I., Sakamoto, M., Ohtsuka, T., Takao, K., Miyakawa, T., Yamaguchi,
946 M., Mori, K., Ikeda, T., Itohara, S., and Kageyama, R. (2008). Roles of
947 continuous neurogenesis in the structural and functional integrity of the adult
948 forebrain. Nat Neurosci 11, 1153-1161.
949 Kempermann, G., Kuhn, H.G., and Gage, F.H. (1997). More hippocampal
950 neurons in adult mice living in an enriched environment. Nature 386, 493-495.
951 Kim, M.D., Jan, L.Y., and Jan, Y.N. (2006). The bHLH-PAS protein Spineless is
952 necessary for the diversification of dendrite morphology of Drosophila dendritic
953 arborization neurons. Genes Dev 20, 2806-2819.

eNeuro Accepted Manuscript

954 Kimura, E., Ding, Y., and Tohyama, C. (2016). AhR signaling activation disrupts
955 migration and dendritic growth of olfactory interneurons in the developing
956 mouse. Sci Rep 6, 26386.
957 Kimura, E., Kubo, K.I., Endo, T., Nakajima, K., Kakeyama, M., and Tohyama, C.
958 (2017). Excessive activation of AhR signaling disrupts neuronal migration in the
959 hippocampal CA1 region in the developing mouse. J Toxicol Sci 42, 25-30.
960 Kimura, E., and Tohyama, C. (2017). Embryonic and Postnatal Expression of
961 Aryl Hydrocarbon Receptor mRNA in Mouse Brain. Front Neuroanat 11, 4.
962 Latchney, S.E., Hein, A.M., O'Banion, M.K., DiCicco-Bloom, E., and
963 Opanashuk, L.A. (2013). Deletion or activation of the aryl hydrocarbon receptor
964 alters adult hippocampal neurogenesis and contextual fear memory. J
965 Neurochem 125, 430-445.
966 Lopez-Rojas, J., and Kreutz, M.R. (2016). Mature granule cells of the dentate
967 gyrus--Passive bystanders or principal performers in hippocampal function?
968 Neurosci Biobehav Rev 64, 167-174.
969 Mandal, P.K. (2005). Dioxin: a review of its environmental effects and its aryl
970 hydrocarbon receptor biology. J Comp Physiol B 175, 221-230.
971 Mimura, J., and Fujii-Kuriyama, Y. (2003). Functional role of AhR in the
972 expression of toxic effects by TCDD. Biochim Biophys Acta 1619, 263-268.
973 Mimura, J., Yamashita, K., Nakamura, K., Morita, M., Takagi, T.N., Nakao, K.,
974 Ema, M., Sogawa, K., Yasuda, M., Katsuki, M., and Fujii-Kuriyama, Y. (1997).
975 Loss of teratogenic response to 2,3,7,8-tetrachlorodibenzo-p-dioxin (TCDD) in
976 mice lacking the Ah (dioxin) receptor. Genes Cells 2, 645-654.
977 Mulero-Navarro, S., and Fernandez-Salguero, P.M. (2016). New Trends in Aryl
978 Hydrocarbon Receptor Biology. Front Cell Dev Biol 4, 45.

eNeuro Accepted Manuscript

979 Murray, I.A., Patterson, A.D., and Perdew, G.H. (2014). Aryl hydrocarbon
980 receptor ligands in cancer: friend and foe. Nat Rev Cancer 14, 801-814.
981 Nakashiba, T., Young, J.Z., McHugh, T.J., Buhl, D.L., and Tonegawa, S. (2008).
982 Transgenic inhibition of synaptic transmission reveals role of CA3 output in
983 hippocampal learning. Science 319, 1260-1264.
984 Nguyen, L.P., and Bradfield, C.A. (2008). The search for endogenous activators
985 of the aryl hydrocarbon receptor. Chem Res Toxicol 21, 102-116.
986 Niv, F., Keiner, S., Krishna, -., Witte, O.W., Lie, D.C., and Redecker, C. (2012).
987 Aberrant neurogenesis after stroke: a retroviral cell labeling study. Stroke 43,
988 2468-2475.
989 Palop, J.J., Chin, J., Roberson, E.D., Wang, J., Thwin, M.T., Bien-Ly, N., Yoo,
990 J., Ho, K.O., Yu, G.Q., Kreitzer, A.*, et al.* (2007). Aberrant excitatory neuronal
991 activity and compensatory remodeling of inhibitory hippocampal circuits in
992 mouse models of Alzheimer's disease. Neuron 55, 697-711.
993 Paoletti, P., Bellone, C., and Zhou, Q. (2013). NMDA receptor subunit diversity:
994 impact on receptor properties, synaptic plasticity and disease. Nat Rev Neurosci
995 14, 383-400.
996 Qin, H., and Powell-Coffman, J.A. (2004). The Caenorhabditis elegans aryl
997 hydrocarbon receptor, AHR-1, regulates neuronal development. Dev Biol 270,
998 64-75.
999 Smith, C.J., O'Brien, T., Chatzigeorgiou, M., Spencer, W.C., Feingold-Link, E.,
1000 Husson, S.J., Hori, S., Mitani, S., Gottschalk, A., Schafer, W.R., and Miller, D.M.
1001 (2013). Sensory neuron fates are distinguished by a transcriptional switch that
1002 regulates dendrite branch stabilization. Neuron 79, 266-280.

eNeuro Accepted Manuscript

1003 Spruston, N., and Johnston, D. (2008). Out of control in the dendrites. Nat
1004 Neurosci 11, 733-734.
1005 Squire, L.R., and Zola-Morgan, S. (1991). The medial temporal lobe memory
1006 system. Science 253, 1380-1386.
1007 Tada, T., and Sheng, M. (2006). Molecular mechanisms of dendritic spine
1008 morphogenesis. Curr Opin Neurobiol 16, 95-101.
1009 van Praag, H., Christie, B.R., Sejnowski, T.J., and Gage, F.H. (1999). Running
1010 enhances neurogenesis, learning, and long-term potentiation in mice. Proc Natl
1011 Acad Sci U S A 96, 13427-13431.
1012 van Praag, H., Schinder, A.F., Christie, B.R., Toni, N., Palmer, T.D., and Gage,
1013 F.H. (2002). Functional neurogenesis in the adult hippocampus. Nature 415,
1014 1030-1034.
1015 Walisser, J.A., Glover, E., Pande, K., Liss, A.L., and Bradfield, C.A. (2005). Aryl
1016 hydrocarbon receptor-dependent liver development and hepatotoxicity are
1017 mediated by different cell types. Proc Natl Acad Sci U S A 102, 17858-17863.
1018 Williamson, M.A., Gasiewicz, T.A., and Opanashuk, L.A. (2005). Aryl
1019 hydrocarbon receptor expression and activity in cerebellar granule neuroblasts:
1020 implications for development and dioxin neurotoxicity. Toxicol Sci 83, 340-348.
1021 Winkle, C.C., Olsen, R.H., Kim, H., Moy, S.S., Song, J., and Gupton, S.L.
1022 (2016). Trim9 Deletion Alters the Morphogenesis of Developing and Adult-Born
1023 Hippocampal Neurons and Impairs Spatial Learning and Memory. J Neurosci
1024 36, 4940-4958.
1025 Woitke, F., Ceanga, M., Rudolph, M., Niv, F., Witte, O.W., Redecker, C., Kunze,
1026 A., and Keiner, S. (2017). Adult hippocampal neurogenesis poststroke: More

eNeuro Accepted Manuscript

1027 new granule cells but aberrant morphology and impaired spatial memory. PLoS
1028 One 12, e0183463.
1029 Yamaguchi, Y., and Miura, M. (2015). Programmed cell death in
1030 neurodevelopment. Dev Cell 32, 478-490.
1031 Zhao, C., Deng, W., and Gage, F.H. (2008). Mechanisms and functional
1032 implications of adult neurogenesis. Cell 132, 645-660.
1033 Zhao, C., Jou, J., Wolff, L.J., Sun, H., and Gage, F.H. (2014). Spine
1034 morphogenesis in newborn granule cells is differentially regulated in the outer
1035 and middle molecular layers. J Comp Neurol 522, 2756-2766.
1036 Zhao, C., Teng, E.M., Summers, R.G., Ming, G.L., and Gage, F.H. (2006).
1037 Distinct morphological stages of dentate granule neuron maturation in the adult
1038 mouse hippocampus. J Neurosci 26, 3-11.
1039 Zhou, M., Li, W., Huang, S., Song, J., Kim, J.Y., Tian, X., Kang, E., Sano, Y.,
1040 Liu, C., Balaji, J., *et al.* (2013). mTOR Inhibition ameliorates cognitive and
1041 affective deficits caused by Disc1 knockdown in adult-born dentate granule
1042 neurons. Neuron 77, 647-654.
1043

1044 **FIGURE LEGENDS**

1045 **Figure 1. Ablation of AhR impairs hippocampus-dependent memory**. **(A)**
1046 Percentage of freezing in the CFC task for $AhR^{+/+}$ and $AhR^{-/-}$ mice 1h (left) and
1047 24h (right) after the foot shocks (*p<0.05 vs. $AhR^{+/+}$; n=8 $AhR^{+/+}$ and 7 $AhR^{-/-}$
1048 animals/group). **(B)** Percentage of exploration time between familiar and new
1049 object in the NOR test for $AhR^{+/+}$ and $AhR^{-/-}$ mice 6h after training. Two-way
1050 ANOVA demonstrated a significant interaction between the object and genotype
1051 [$F_{(1, 18)}$=7,46; p<0.05] (*p<0.05 vs. $AhR^{+/+}$; n=6 $AhR^{+/+}$ and 5 $AhR^{-/-}$
1052 animals/group). **(C)** Percentage of exploration time between old and new object
1053 location in the NOL test for $AhR^{+/+}$ and $AhR^{-/-}$ mice 6h after training. Two-way
1054 ANOVA demonstrated a significant interaction between the object and genotype
1055 [$F_{(1, 42)}$=7.93; p<0.05]; (*p<0.05 vs. $AhR^{+/+}$; n=12 $AhR^{+/+}$ and 11 $AhR^{-/-}$
1056 animals/group). **(D)** Percentage of time spent in each arm in the Y-maze test for
1057 $AhR^{+/+}$ and $AhR^{-/-}$ mice 6h after training. Two-way ANOVA showed a significant
1058 interaction between the arm/genotype [$F_{(2, 27)}$=3.84; p<0.05] (n=6
1059 animals/group). **(E)** Time spent to find the escape box during the Barnes maze
1060 training sessions in both $AhR^{+/+}$ and $AhR^{-/-}$ mice. Two-way ANOVA
1061 demonstrated a significant effect during training sessions [$F_{(5, 65)}$=5.04; p<0.05]
1062 (n=7-8 animals/group). **(F)** Density plots for grouped data showing where the
1063 $AhR^{+/+}$ and $AhR^{-/-}$ mice concentrated their searches during retention test day.
1064 **(G)** Percentage of time spent around each hole (s) in the Barnes maze platform
1065 for $AhR^{+/+}$ and $AhR^{-/-}$ mice during the retention test day. Two-way ANOVA
1066 demonstrated a significant interaction between the holes and genotype [$F_{(19,
1067 260)}$=1.83; p<0.05] (*p<0.05 vs. $AhR^{+/+}$; n=7-8 animals/group). Data are mean ±
1068 SEM. Data were compared by using non-parametric 2-tailed Mann-Whitney test

eNeuro Accepted Manuscript

eNeuro Accepted Manuscript

1069 (A), 2-way ANOVA (B-G) or a nonparametric 2-way ANOVA followed by
1070 Bonferroni post hoc testing (B-E).
1071
1072 **Figure 2. The absence of AhR exacerbates adult hippocampal**
1073 **neurogenesis. (A)** $BrdU^+$ cells in the DG of $AhR^{+/+}$ and $AhR^{-/-}$ mice measured
1074 at p30, p60 and p100 24h after the last BrdU injection. Two-way ANOVA
1075 demonstrated a significant interaction between the age and genotype [$F_{(2,}$
1076 $_{24)}$=9.51; p<0.05] (*p<0.05 vs. $AhR^{+/+}$; n=5 animals/group). **(B-C)** $Ki67^+$ cells in
1077 the DG of $AhR^{+/+}$ and $AhR^{-/-}$ mice measured at p30, p60 and p100. Two-way
1078 ANOVA demonstrated a significant interaction between the age and genotype
1079 [$F_{(2, 28)}$=8.56; p<0.05] (*p<0.05 vs. $AhR^{+/+}$; n=5-6 animals/group). Representative
1080 images of $Ki67^+$ cells in $AhR^{+/+}$ and $AhR^{-/-}$ mice at different time points are
1081 shown in (C). **(D-F)** Quantification of the number of nestin/$BrdU^+$ cells by flow
1082 cytometry 24h after BrdU administration. Data are expressed as the percentage
1083 of control group (*p<0.05 vs. $AhR^{+/+}$; n=6 animals/group) (D). Representative
1084 dot plots of double-stained cells for nestin and BrdU in the DG of $AhR^{+/+}$ (E) and
1085 $AhR^{-/-}$ (F) mice. **(G-L)** Characterization of type-1 ($nestin^+$/$GFAP^+$) (G) and type-2
1086 progenitors ($nestin^+$/$GFAP^-$) (I) and their proliferative capacity ($BrdU^+$) (H and J)
1087 in the DG of $AhR^{+/+}$ and $AhR^{-/-}$ mice determined at p30 and p100.
1088 Representative images of nestin (red), GFAP (green), BrdU (grey) of DG of
1089 $AhR^{+/+}$ and $AhR^{-/-}$ mice at p30 (K) and p100 (L) (*p<0.05 vs $AhR^{+/+}$; #p<0.05 vs
1090 $AhR^{-/-}$; n=4-6 animals/group). **(M-N)** Quantification of the number of DCX^+ cells
1091 in the DG of WT and $AhR^{-/-}$ mice (*p<0.05 vs. $AhR^{+/+}$; n=7-8 animals/group).
1092 Representative images of DCX^+ cells in $AhR^{+/+}$ and $AhR^{-/-}$ mice are shown in
1093 (N). **(O-P)** Quantification of the number of $BrdU^+$ cells (left) and newborn

1094 integrated neurons (BrdU$^+$/Calbindin$^+$) (right) determined 28 days after BrdU
1095 administration (*$p<0.05$ vs. AhR$^{+/+}$; n=7-9 animals/group). Representative co-
1096 localisation images for BrdU and calbindin in AhR$^{+/+}$and AhR$^{-/-}$ mice are shown
1097 in (P). Insets display high magnifications images. Numbers of cells are
1098 expressed per 1000 μm^2. Data are mean ± SEM. Scale bar is 50μm in C and K-
1099 L and J, 70μm in N, 30μm in P. Data were compared by using non-parametric
1100 2-tailed Mann-Whitney test in D, M and O or a non-parametric 2-way ANOVA
1101 followed by Bonferroni post hoc testing (A, B, G-J).
1102

1103 **Figure 3. The absence of AhR alters granule cells morphology and**
1104 **dendritic spine density and maturation. (A)** Sholl analysis of granule
1105 dendritic branching of Golgi-Cox stained DG from AhR$^{+/+}$ and AhR$^{-/-}$ p60 mice.
1106 Two-way ANOVA demonstrated a significant interaction between
1107 distance/genotype [$F_{(24, 125)}=2.45$; $p<0.05$]; (*$p<0.05$ vs. AhR$^{+/+}$) (n=23 WT and
1108 37 AhR KO neurons from 3-4 animals/group). Representative reconstructions of
1109 Golgi-Cox stained neurons are shown for AhR$^{+/+}$ (left) and AhR$^{-/-}$ mice (right).
1110 **(B)** Total dendritic length of Golgi-Cox-stained granular cells (*$p<0.05$ vs. AhR).
1111 **(C)** Quantification of spine density in Golgi-Cox stained neurons (*$p<0.05$ vs.
1112 AhR$^{+/+}$; n=20-30 dendrite segments from 3-4 animals/group). **(D)** Densitometric
1113 analysis of dendrite DCX$^+$ labelling distribution in the DG of WT and AhR$^{-/-}$ mice
1114 at p60. Data is displayed as the DCX$^+$ integrated density found in total
1115 (GL+ML), GL or ML normalized by values got from soma. (E) Quantification of
1116 apical neuroblast length. Representative images of DCX$^+$ labelling distribution in
1117 AhR$^{+/+}$ and AhR$^{-/-}$ mice are shown in (F). (*$p<0.05$ vs. AhR$^{+/+}$; n=5-6
1118 animals/group). **(G-N)** GFP-retroviral infection of newborn neurons. Schematic

eNeuro Accepted Manuscript

eNeuro Accepted Manuscript

1119 protocol followed for CAG-GFP retrovirus infusion in $AhR^{+/+}$ and $AhR^{-/-}$ p60 mice
1120 (G). Representative GFP newborn $AhR^{+/+}$ (left) and $AhR^{-/-}$ neurons (right) are
1121 shown in (H). Two-way ANOVA of Sholl analysis in GFP-labelled dentate
1122 granule cells demonstrates a significant interaction between the distance and
1123 genotype [$F_{(4,30)}$=3.02; p<0.05]; (*p<0.05 vs. $AhR^{+/+}$; n=19 WT and 28 AhR KO
1124 neurons from 4 animals/group; I). Quantification of total dendritic length (J) and
1125 apical dendritic length (K). Density of dendritic (L) and mushroom spines (M) in
1126 proximal and distal dendritic segments in the molecular layer of $AhR^{+/+}/GFP^{+}$
1127 and $AhR^{-/-}/GFP^{+}$ granule cells 4 weeks post-infection (*p<0.05 vs. $AhR^{+/+}/GFP^{+}$;
1128 n=26 and 22 segments from 4 animals/group). Representative images of GFP-
1129 labelled spines in both proximal and distal segments of $AhR^{+/+}/GFP^{+}$ and $AhR^{-/-}$
1130 $/GFP^{+}$ granule cells (N). Insets display high magnifications images. Data are
1131 mean ± SEM. Data were compared by using non-parametric Mann-Whitney
1132 tests in B-C, D-E and J-M or a non-parametric 2-way ANOVA followed by
1133 Bonferroni post hoc testing (A and I). Scale bar is 70μm in F and H, and 2μm in
1134 O.
1135
1136 **Figure 4. AhR deletion alters the synaptic properties of dentate gyrus**
1137 **granule cells. (A)** Schematic representation of a hippocampal slice showing
1138 stimulating and recording electrode sites. **(B-C)** The resting membrane potential
1139 (B) and the current-voltage relationship (C) were not significantly different
1140 between DG granule cells from $AhR^{+/+}$ and $AhR^{-/-}$ mice (n=4 animals/group). **(D-**
1141 **E)** DG granule cells firing rate is significantly increased by AhR deletion
1142 (*p<0.05 vs. $AhR^{+/+}$). Representative sample traces (D) and averaged values
1143 (E) in response to increasing depolarising currents. **(F-G)** AMPA/NMDA ratio is

eNeuro Accepted Manuscript

1144 decreased by AhR deletion (*$p<0.05$ vs. $AhR^{+/+}$). Representative traces (F) and
1145 averaged values (G) of NMDA- and AMPA-mediated EPSCs recorded at +40
1146 and -60 mV, respectively. **(H)** Averaged values showing a significant increase in
1147 the PPR at interstimulus intervals of 75, 100, 150 and 200 ms in cells lacking
1148 AhR (*$p<0.05$ vs. $AhR^{+/+}$. EPSC sample traces represent the mean of 20
1149 consecutive EPSCs at 0.33Hz. Data are mean ± SEM (14 neurons from 8 slices
1150 from n=4 $AhR^{+/+}$ mice and 12 neurons from 8 slices from n=4 $AhR^{-/-}$ mice). Data
1151 were compared by using non-parametric 2-tailed Mann-Whitney tests.

1152

1153 **Figure 5. Acute ablation of AhR in adult neural precursors impairs**
1154 **hippocampus-dependent memory by promoting aberrant immature**
1155 **neurons. (A)** Schematic diagram of the strategy for conditional deletion of AhR
1156 in NPCs in nestin-$Cre^{ERT2+/}AhR^{f/f}$ mice (AhR-icKO). $AhR^{f/f}$ and nestin-
1157 $Cre^{ERT2+/}AhR^{f/f}$ mice were administered two rounds of tamoxifen (TAM; at p30
1158 and p60) at a dose of 180mg/Kg. **(B)** AhR immunostaining in $AhR^{f/f}$ (left) and
1159 AhR-icKO (right) 3 weeks after the second round of TAM
1160 injection. **(C)** Quantification of the number of DCX^+ cells per 1000 μm^2. in the
1161 DG of $AhR^{f/f}$ and AhR-icKO mice 3 weeks after the last TAM injection (*$p<0.05$
1162 vs. $AhR^{f/f;}$ n=8-8 animals/group) (left). Representative images of DCX^+ staining
1163 in $AhR^{f/f}$ and AhR-icKO mice (right). **(D)** Densitometric analysis of dendrite
1164 DCX^+ labelling distribution in the DG of $AhR^{f/f}$ and AhR-icKO mice 3 weeks after
1165 the last TAM injection. Data is displayed as the DCX^+ integrated density found
1166 in total (GL+ML), GL or ML normalized by values got from soma (*$p<0.05$ vs.
1167 $AhR^{f/f}$; n=6 $AhR^{f/f}$ and 5 AhR-icKO animals/group) (left). Representative images
1168 of the arborisation of immature newborn cells in $AhR^{f/f}$ and AhR-icKO mice

eNeuro Accepted Manuscript

1169 (right). **(E)** Protocol followed for a weak contextual fear conditioning paradigm
1170 (0.4mA x1) in AhR$^{f/f}$ and AhR-icKO treated with tamoxifen. Retrieval was
1171 performed 24h after training. (*$p<0.05$ vs AhRf/f; n=10-11 animals/group). **(F)**
1172 Percentage of time spent in each arm in the Y-maze test for AhR$^{f/f}$ and AhR-
1173 icKO mice 3 weeks after the last TAM injection 6h after training. Two-way
1174 ANOVA demonstrated a significant interaction between the arm and genotype
1175 [$F_{(2, 57)}=5.91$; $p<0.05$] (n=10-11 animals/group). **(G)** Percentage of exploration
1176 time between old and new object location in the NOL test for AhR$^{f/f}$ and AhR-
1177 icKO mice 3 weeks after the last TAM injection 6h after training (n=10-11
1178 animals/group). Data are mean ± SEM. Scale bar is 50μm in B, C and D. Data
1179 were compared by using non-parametric 2-tailed Mann-Whitney test (C-E), or a
1180 non-parametric 2-way ANOVA followed by Bonferroni post hoc testing (F-G).
1181

1182 **Figure 6. Acute ablation of AhR in adult neural precursors alters the**
1183 **synaptic properties of dentate gyrus granule cells. (A)** Experimental
1184 protocol for tamoxifen administration and electrophysiological recordings. **(B-C)**
1185 The resting membrane potential (B) and the current-voltage relationship (C) did
1186 not show significant differences between DG granule cells from AhR$^{f/f}$ and AhR-
1187 icKO mice (n=4-6 animals/group). **(D-E)** DG granule cells firing rate is
1188 significantly increased by specific AhR ablation (*$p<0.05$ vs. AhR$^{f/f}$).
1189 Representative sample traces (D) and averaged values (E) in response to
1190 increasing depolarising currents. **(F-G)** AMPA/NMDA ratio is decreased by AhR
1191 deletion (*$p<0.05$ vs. AhR$^{f/f}$). Representative traces (F) and averaged values (G)
1192 of NMDA- and AMPA-mediated EPSCs recorded at +40 and -60 mV,
1193 respectively. **(H)** Averaged values showing a significant increase in the PPR at

1194 interstimulus 75, 100, 150 and 200-ms intervals in cells lacking AhR (*p<0.05

1195 vs. $AhR^{f/f}$). Data are mean ± SEM (25 neurons from 8 slices from n=6 $AhR^{f/f}$

1196 mice and 24 neurons from 8 slices from n=4 AhR-icKO mice). Data were

1197 compared by using non-parametric 2-tailed Mann-Whitney tests.

eNeuro Accepted Manuscript

eNeuro Accepted Manuscript

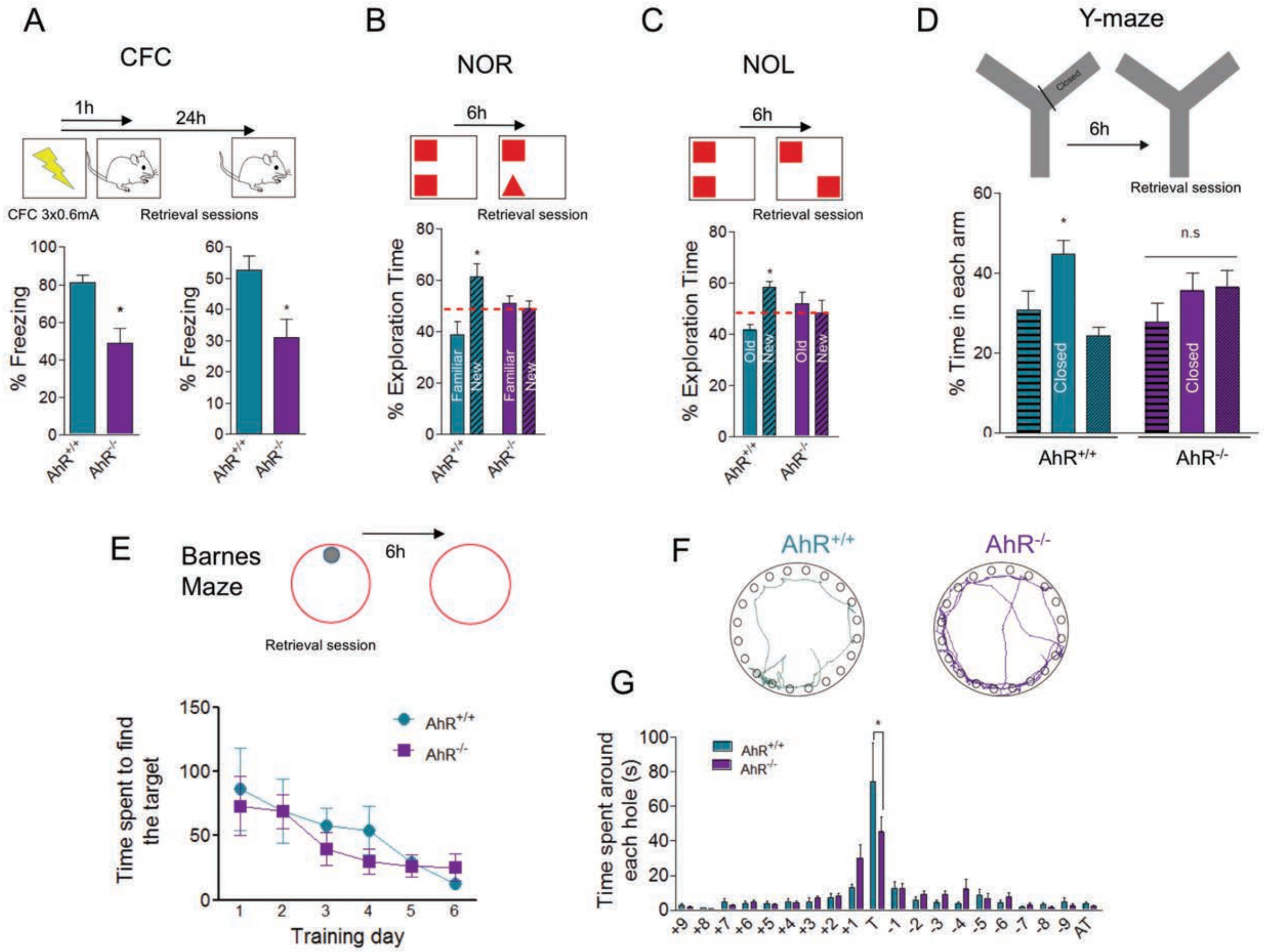

eNeuro Accepted Manuscript

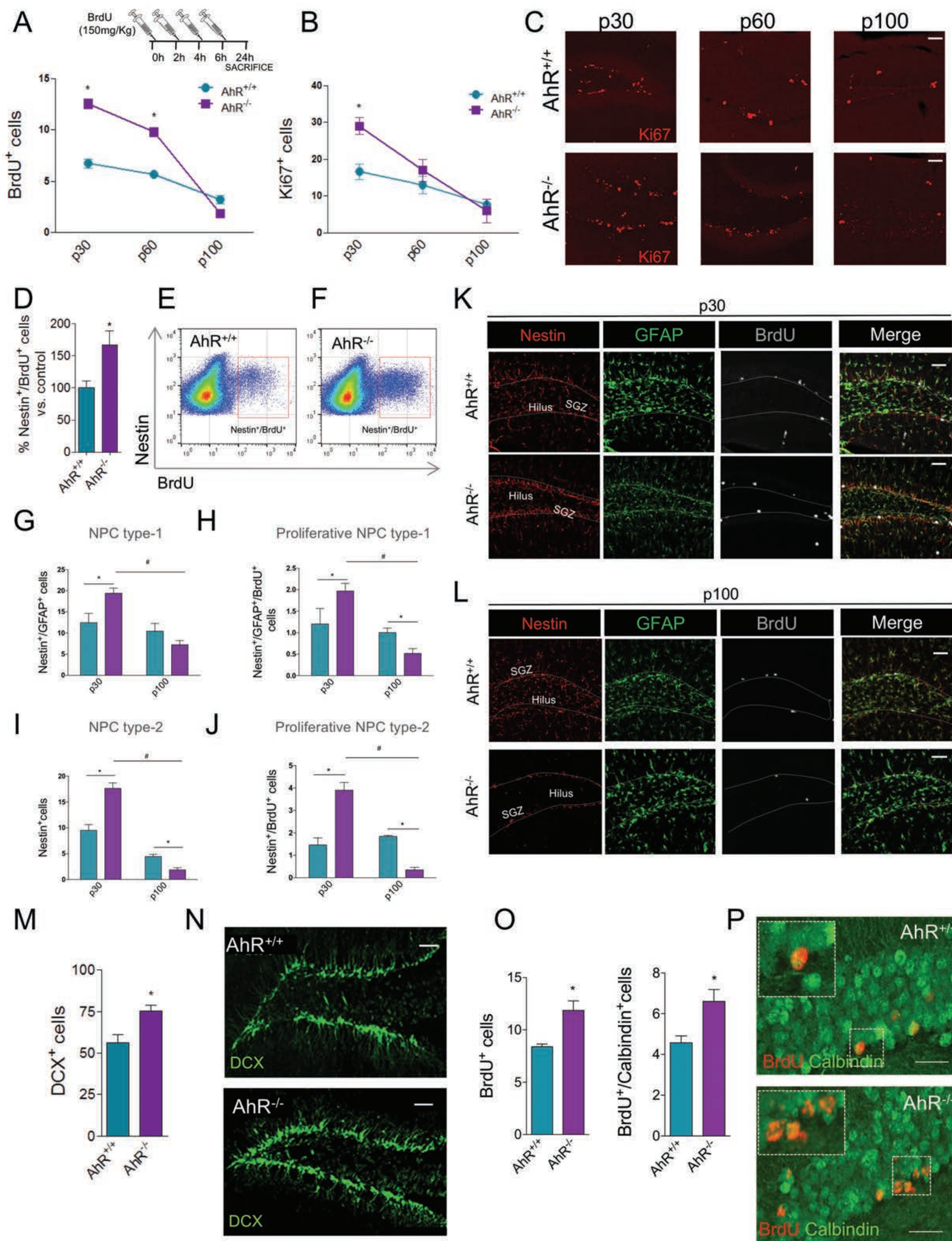

eNeuro Accepted Manuscript

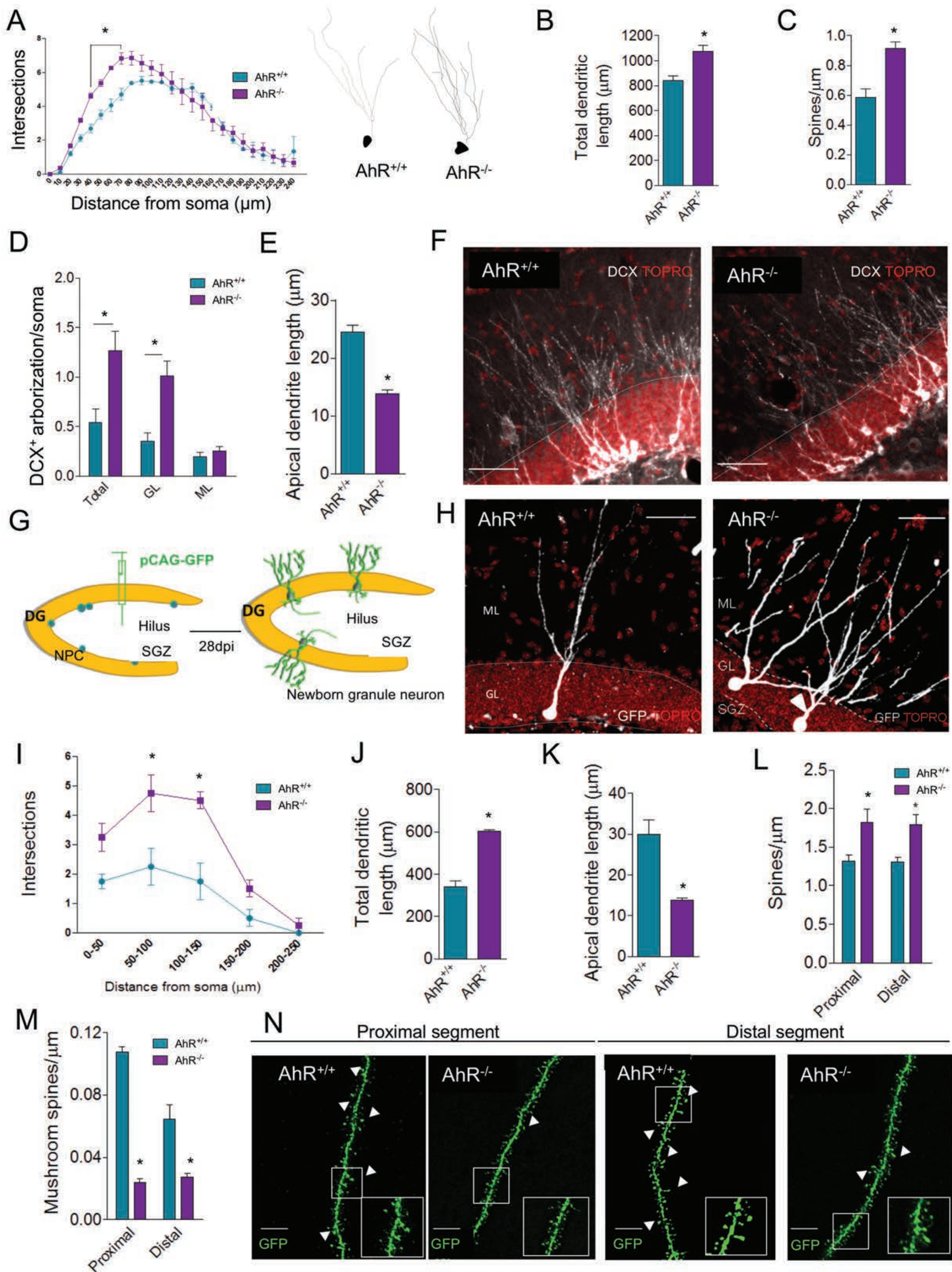

eNeuro Accepted Manuscript

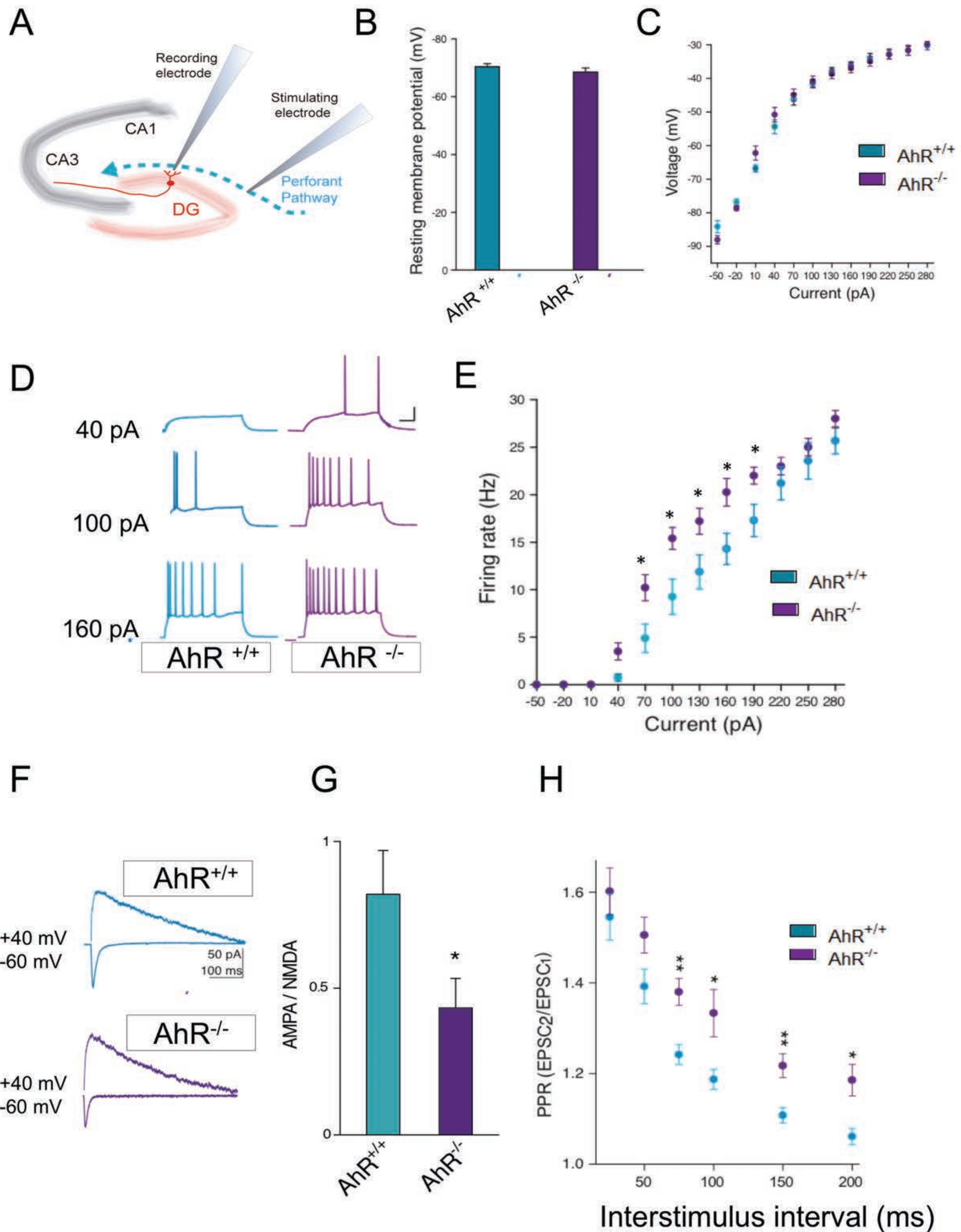

eNeuro Accepted Manuscript

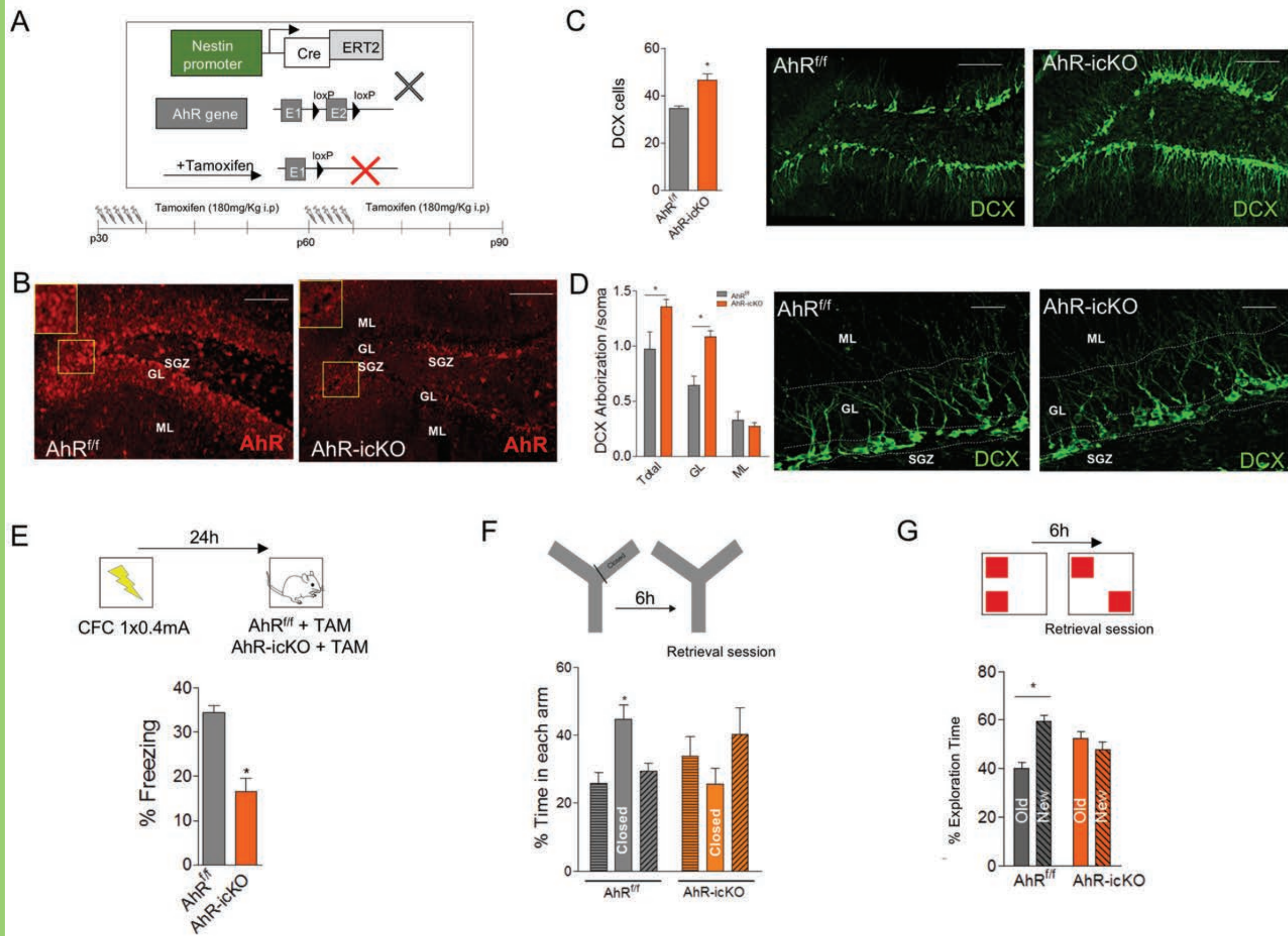

eNeuro Accepted Manuscript